

# Finite element analysis of thermal fields during repair welding of discrete rail defects

Master's Thesis in Applied Mechanics, Chalmers Tekniska Högskola

MICHELE MARIA MAGLIO



MASTER'S THESIS IN APPLIED MECHANICS

Finite element analysis of thermal fields during repair  
welding of discrete rail defects

MICHELE MARIA MAGLIO

Department of Applied Mechanics  
Division of Dynamics  
CHARMEC  
CHALMERS UNIVERSITY OF TECHNOLOGY  
Göteborg, Sweden 2017

Finite element analysis of thermal fields during repair welding of discrete rail defects

MICHELE MARIA MAGLIO

© MICHELE MARIA MAGLIO, 2017-06-12

Supervisor: Elena Kabo  
Examiner: Anders Ekberg

Master's Thesis 2017:17  
ISSN 1652-8557  
Department of Applied Mechanics  
Division of Dynamics  
CHARMEC  
Chalmers University of Technology  
SE-412 96 Göteborg  
Sweden  
Telephone: + 46 (0)31-772 1000

Cover:  
Snap shot of evaluated temperatures during discrete defect repair welding

CHARMEC / Department of Applied Mechanics  
Göteborg, Sweden 2017-06-12

Finite element analysis of thermal fields during repair welding of discrete rail defects

Master's thesis in Applied Mechanics, Chalmers University of Technology

Master's thesis in Mechanical Engineering, Politecnico di Torino

MICHELE MARIA MAGLIO

Department of Applied Mechanics

Division of Dynamics

CHARMEC

Chalmers University of Technology

## **Abstract**

Discrete defects in a rail head may form due to aggressive wheel–rail contact in terms of thermal and/or mechanical loads, or due to indentations from foreign objects trapped in the contact. If large, such defects need to be repaired or the rail section removed. These are costly operations that cause operational disturbances. To decrease mitigation costs, discrete defect repair (DDR) procedures that include repair welding have been developed. These operations typically require high preheat temperature (350 °C) and long working process times.

This MSc-thesis work investigates a novel DDR rail welding procedure through numerical simulations. The new technique employs significantly lower preheat temperature (60–80 °C) and equipment that can easily be carried to the working place. However, the low preheating temperature introduces high temperature differences between the molten filler material and the surrounding rail steel. This may lead to the formation of defects, welding related cracks or martensitic areas.

The aim of the work is to simulate the DDR procedure and thereby be able to analyse the thermal history in the rail during the welding process. In this manner, cooling curves for critical locations in the rail head can be evaluated and the risk of weld related defects and metallurgical transformations to hard microstructures can be assessed. To achieve these ends, numerical models of a milled rail head were created in ABAQUS/CAE. The repair welding procedure was then simulated and the results compared to experimental data from the literature.

The results show temperature trends that are in line with temperature measurements from trials carried out some years ago. The simulations show the sensitivity to parameters such as the temperature of the molten filler and cooling times. There is thus a high potential in simulating operational procedures and thereby be able to e.g. investigate effects of various process parameters. However, to this end more high-quality test data are required. In particular the simulations show how sensitive a calibration is to the exact position of thermocouples. On the other hand, the simulations performed in the thesis have shown that small variations in the geometry of the numerical model of the repair process do not have a significant influence on the predicted cooling curves.



# Contents

Abstract.....	I
Contents.....	III
Preface.....	V
Notations.....	VI
1 Repair welding.....	1
1.1 Wheel-rail rolling contact and discrete defects.....	1
1.2 Discrete defect repair methods.....	2
1.2.1 Rail replacement.....	3
1.2.2 Manual Metal Arc (MMA) repair.....	3
1.2.3 Flux Cored Arc Welding (FCAW).....	3
1.2.4 Wide gap aluminothermic weld.....	3
1.2.5 Flash butt wedge repair.....	4
1.2.6 Thermit Head Repair (HR).....	4
1.3 British Steel DDR process.....	5
1.4 Results from trials.....	7
2 Scope & aims.....	10
3 FE-model.....	12
3.1 Geometry.....	12
3.1.1 Rail.....	12
3.1.2 Cavity.....	13
3.2 Boundary conditions.....	16
3.3 Material properties.....	18
3.3.1 Rail material.....	18
3.3.2 Filler material.....	19
3.4 Discretisation.....	20
3.4.1 Weld beads.....	20
3.4.2 Finite element mesh.....	22
3.5 Modelling of the welding process.....	23
3.5.1 Weld definition.....	23
3.5.2 Pass and job definition.....	24
3.5.3 Temporary boundary conditions.....	24
3.5.4 Intercooling steps.....	25
3.5.5 Thermal fluxes.....	25
4 Results.....	27

4.1	Sensitivity analysis .....	27
4.2	Robustness analysis .....	29
4.3	Thermal history results .....	31
4.3.1	Influence of the filler material temperature .....	32
4.3.2	Influence of the thermocouple position .....	35
4.3.3	Influence of the corner geometry .....	40
5	Conclusions.....	43
6	Future work.....	46
7	Acknowledgements.....	47
	References .....	48
	Appendix A – Sensitivity analysis.....	50
A1	Central Point.....	50
A2	Right point.....	51

## **Preface**

I would like to say thank you to my supervisor Elena Kabo for all the suggestions and support she has given to me in these five months. It was a real pleasure for me to work with her on the first “real engineering” project of my career. I would also like to thank her for making me aspire to perfection and professionalism in this work and for teaching me to tackle problems “sakta men säkert”.

Thanks to my examiner Anders Ekberg for recommending this Master Thesis project to me, for providing me with all the literature material I needed and for all the precious suggestions, feedback and recommendations he gave on the analysis procedures and on the results.

I am grateful to both Elena and Anders for being so kind to me and for revising this report and giving a lot of suggestions on the content and the style, thus making it look much more professional and effective.

A huge thank you goes to all my Family members who have always made me feel their love and enthusiasm even if I was very far from home, at first in Turin and then in Gothenburg. They encouraged, supported and cheered me up in all the moments of my studies and they gave me strength when I was worried by exams or deadlines. A special thought goes to my beloved grandmother who passed away during this exchange year.

I would like to show my thankfulness to all the relatives and friends who visited me in Sweden this year. Thanks to my friends of a lifetime, the ones from Maglie and nearby, that I am always longing to meet again when I am away and with whom it is nice to have a chat when I am homesick. I also feel lucky to have met so many nice people in Gothenburg who made this Erasmus year so special and I would like to say thank you to them all and especially to the ones with whom I spent these fantastic five months of MSc thesis work.

Finally, I want to say thank you to my Turin “university projects friends” and to the people I had the privilege to meet on the third floor of Collegio Einaudi: After sharing hopes and worries, opinions and meals, lectures and holidays, exam sessions and party evenings for four years I really feel like I owe them a significant share of my academic achievements. They turned up to be my second big family from the rest of the world: I really wish I will keep in touch with them for the rest of my life.

MICHELE MARIA MAGLIO

## Notations

AWI	Abaqus Welding Interface
BC	Boundary Conditions
DDR	Discrete Defect Repair
DOF	Degrees of Freedom
FCAW	Flux Cored Arc Welding
FE	Finite Element
HAZ	Heat Affected Zone
MMA	Manual Metal Arc repair
RCF	Rolling Contact Fatigue

# 1 Repair welding

## 1.1 Wheel–rail rolling contact and discrete defects

In railway applications, the rolling contact between the wheel and the rail is expected to cause material degradation in form of wear, rolling contact fatigue and possibly plastic deformations. This will lead to rail deterioration and eventually reduce the load carrying capacity of the rail. The contact behaviour of the mating surfaces is quite complex and unpredictable, and the rolling contact may lead to the formation of different discrete defects which can result in a substantial shortening of the rail life [1].

The most frequent kinds of discrete defects that can be found on many mixed-traffic railway networks are squats and wheel burns [2]. Examples of these damage types are shown in Figure 1.1.



*Figure 1.1 – Rail surface affected by squats (picture courtesy A. Ekberg)*

A squat is a local rolling contact fatigue. The creation of squats is a complex and not fully understood phenomenon where the contact stresses between wheel and rail is a key parameter, cf [3]. Cracks from squats grow in from the surface and degrade the rail head material.

Wheel burns are caused by slipping of wheels on rails [4]. The friction associated with the relative motion creates a very hot area which is rapidly cooled as the wheel moves away. This may cause the formation of a hard and brittle martensite layer on the rail surface.

There are a multitude of other kinds of damage types that may affect the rail head, see [5] and [6], however the above are the most common causes to discrete defects, which are the topic of the current thesis.

Even though most of the discrete damage areas are actually quite shallow and do not individually represent a threat to the rail integrity, it should be borne in mind that a frequent presence of them can eventually cause failures in the track as cracks form and grow from the discrete defects. When it comes to selecting a mitigating action, it

should be considered that substituting the entire rail is costly, requires significant time in track and introduces two cuts and welds to mount the replaced rails.

This is the reason why Discrete Defect Repair (DDR) methods are currently being investigated. These procedures involve an initial phase in which the worn part of the rail is trimmed away. After that, the original geometry is restored by filling the cavity with weld material and then grinding off excessive material.

## 1.2 Discrete defect repair methods

The work in this section relates strongly to the overviews in references [1], [2], [7] and [8], where further details may be found.

As discussed in the previous section, the presence of small defects can pose a potential risk for the integrity of the rail. Sometimes squats, wheel burns, etc. are clearly visible on the rail surface, whereas in other cases some more advanced inspection systems are required (e.g. magnetic inspection, ultrasound, etc.).

Appropriate actions are needed if defects are present. The replacement of the whole rail, as anticipated above, implies high costs and the need to distribute replacement rail to the site. The replacement rail then has to be mounted by means of cutting up the damaged part, replacing it and welding the new rail. The procedure should be carried out in a manner that avoids the introduction of vertical and lateral irregularities, and so-called “cupping” (local plasticity/wear close to the weld). Any such irregularities on the running surface of the rail causes faster degradation of the track due to the higher dynamic forces caused by local increases in the wheel–rail contact. Further it has to be ensured that the rail replacement does not affect the stress free temperature of the rail.

Although clear statistics are not available, the main European railway networks have to remove on average 0.48 defects per British mile of track per year [7]. It is thus clear that some alternative and cost-effective methods for the repair of discrete defects would be desirable. In particular, such techniques should allow a robust and reliable in-situ repair. Rapidity is another requirement since there is a strong desire among infrastructure managers to minimise the time in which the track availability is reduced in order to avoid delays or re-routing of train operations.

Different processes have been proposed for DDR, several of which are currently in use in the railway industry [2]. However, these procedures can differ significantly in the way they are performed, in the type of equipment that is required and in the metallographic structure of the repaired material. Some of these techniques are quite new, so no reliable control on the behaviour of the repaired area has been performed yet. Moreover, although some DDR processes were introduced in the railway track industry as early as in the 1920s [2], it was not until some years ago that major infrastructure managers started to approve them [2].

These are the reasons why the EU project *In2Rail* aims, among other things, at developing and evaluating different techniques for the repair of rail head defects, thus providing a benchmark to compare the efficiency of the different procedures.

Some of the most common DDR mitigation techniques in Europe are briefly described in the following sections.

### **1.2.1 Rail replacement**

This method basically consists in replacing the defected rail with a new one. A replacement rail of at least 5 metres is usually required for such a replacement [8], [9].

As discussed above, this procedure is costly, time consuming and requires cutting and two vertical aluminothermic welds, which can cause further deterioration<sup>1</sup>. These are the reasons why this option is conveniently applicable only if the defected rail is close to the end of its life cycle.

### **1.2.2 Manual Metal Arc (MMA) repair**

In this procedure (often referred to as Shield Metal Arc Welding), the defect is manually excavated by milling. The resulting cavity is subsequently refilled using manual metal arc techniques. The preheating temperature is at least 343°C and other parameters depend on the manufacturers' expertise [2].

Although this process is well established and generally robust, the correct outputs of the grinding and welding procedures depend on the ability of the welder. The whole procedure takes up to 4 hours. Among other downsides, there may be inconsistencies in the heat affected zone microstructure which can significantly shorten the fatigue life of the metal.

The industry has recently standardised the procedures and the consumables and has introduced assessment of the welder ability (standard EN 287-1) [2].

### **1.2.3 Flux Cored Arc Welding (FCAW)**

This process is similar to MMA, but the welding operation is semi-automatic. The heat is given by an arc between the continuous electrode wire and the work piece. The flux cored electrode creates a slag layer which has to be brushed away manually.

The grinding phase is still manual, therefore the output does depend on the operator ability.

### **1.2.4 Wide gap aluminothermic weld**

This technique is basically an extension of the aluminothermic welding process. This allows the welder to use an established technology but, as a consequence, the downsides of the casting technology are extended to weld (i.e. large heat affected zone, change in residual stresses, poor automation, cumbersome transportation of the equipment) [8].

---

<sup>1</sup> Note that all repair methods will introduce welds, in many cases larger than the aluminothermic welds, so this is not a unique problem for rail replacements.

### 1.2.5 Flash butt wedge repair

This process consists in welding a wedge of rail material into a slot which has been carved out to remove the defect, as shown in Figure 1.2. The internal integrity of the wedge gives excellent mechanical properties, but the procedure is complex and not well established according to [8].



Figure 1.2 – Carved slot (left) and completed flash butt weld (right) [8]

### 1.2.6 Thermit Head Repair (HR)

In this process, the defect is excavated using a cutting torch guided by a template. The resulting slot is then filled by means of casting in a specifically designed mould. This allows the removal of deeper defects and to work with overlapping repairs [8]. The resulting large cast structure might have a different wear resistance as compared to the original rail. Further, the repair equipment, as shown in Figure 1.3, is quite complex according to [8].



Figure 1.3 – HR process – mould preparation (left) and preheating phase (right) [2]

To be more specific, there are two different types of HR [2]:

- Head Repair Weld (HRW) (also known as Thermit Head Repair (THR))
- Head Wash Repair (HWR)

These two processes do not differ much in the defect detection and removal phases. Torch excavation is more common in the HRW process, whereas grinding is used in for HWR.

Preheating, the use of moulds and the pouring phases are common in the two methods, but different parameters are used. Different techniques for grinding and final testing have been developed too.

### 1.3 British Steel DDR process

The key characteristics of this process are the minimisation of the human interference and the very low preheat temperatures in comparison with other DDR methods [10]. To facilitate transportation and repair times, a single frame on which all the necessary equipment is mounted has been developed.

In this method, the defect is removed and a weld cavity is prepared by means of a computer controlled milling procedure. The cut-out is 100 mm long, 10 mm deep and it covers the full width of the rail head (72 mm). Its shape is seen in Figure 1.4.



Figure 1.4 – Milled cavity [7]

One characteristic of this procedure is the use of a prototype unit in which the laser guidance, the milling tool and the FCAW welding head are all mounted. The unit is designed in such a way that it is easily possible to transport it to the place in which the repair procedure has to be performed, see Figure 1.5.



Figure 1.5 – Prototype unit employed during the DDR tests [10]

Before proceeding with welding operations, a preheat temperature of 80°C is applied to the rail. This preheat is considerably lower compared to other DDR welding techniques (where it is greater than 343°C). The use of such a low temperature eliminates the need for time consuming preheating to higher temperatures whilst preventing the completion of the transformation to martensite and retaining austenite. The deposition of subsequent beads tempers the martensite to a tough microstructure. In the case of the analysed DDR process, the weaved pattern permits the transformation to pearlite. In the penultimate layer, the start and end edges of the

cavity can create a HAZ that is susceptible to martensite formation but that can be tempered by a top sacrificial layer. [10][16]

The welding procedure is carried out as a semi-automatic open arc welding process under the guidance of a laser system. The consumable is deposited following a square weave pattern which, in this DDR procedure, is always perpendicular to the rail longitudinal direction [11]. The beginning of the path can be seen in Figure 1.6.

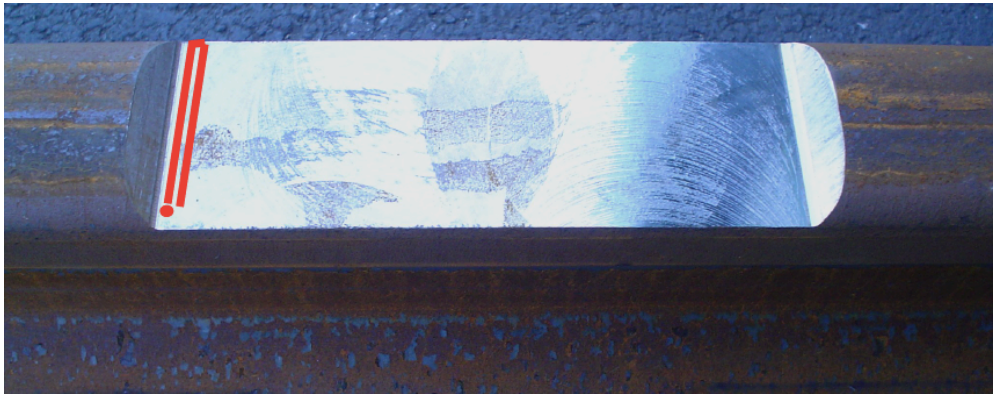


Figure 1.6 – The first part of the welding path [14]

Three layers are sufficient to cover the whole cavity, as shown in Figure 1.7, although a fourth sacrificial layer is used to ensure that the whole HAZ is tempered. Some time is spent after each layer deposition in order to manually remove slag using a pinning gun. This time frame allows the rail base material and the welding metal to cool down to an extent before a new layer is deposited.

The process is concluded with a manual grinding procedure in which the original rail head geometry is restored, see Figure 1.8. The efficiency of the grinding process is ensured by smoothness measurements on the restored surface and a visual inspection of the repaired rail.



Figure 1.7 – Appearance of the repaired area after the third layer is laid [10]



Figure 1.8 - Appearance of the repaired area after grinding [10]

## 1.4 Results from trials

Three sets of experiments were carried out in York, UK, in June 2016. Two of these experiments failed, the failure was due in one case to a problem with the software controlling the equipment and in the other case to an accumulation of spatter around the welding nozzle [10].

Since the aim of this report is to study the thermal effects of the whole welding procedure, the simulations will be based on results obtained in the third set. Normally four layers are deposited but on the experiment in June 2016 just three layers were used for the third experimental set [17].

As reported in Table 1.1, the preheating phase was accomplished in about 10 minutes by using an oxy/propane preheater. After that, the deposition phase, which used a 1.6 mm flux cored wire, started. The adopted consumable was named ESAB Tubrod 15.43, but it has lately been rebranded as ESAB Tubrodur 35 OM.

The rail was made of R260 steel. It took around 4 minutes to complete the weld run of each layer (slightly more for the third layer) and the slag removal phases in-between the different passes took about 3 minutes each.

The recorded rail temperatures during the DDR attempt are listed in Table 1.1 and are presented in the form of a graph in Figure 1.9.

DDR Process	total process time		sequence time	weld time	rail temperature -deg C	
	actual	elapsed			A	B
DDR weld 3	hr.min.sec	mins	mins	elapsed (s)		
Process start					16	17
Milling start	14.17.30	0.00			16	17
Milling finish	14.32.45	15.25	15.25		32	33
Preheat start	14.38.45	21.25		0.00	30	30
Preheat finish	14.48.50	31.34	10.09	605.40	120	90
Weld run 1- start	14.50.00	32.50		675.00	120	100
Weld run 1- finish	14.54.00	36.50	4.00	915.00	190	160
Weld run 2 - start	14.56.50	39.34		1085.40	190	160
weld run 2 - finish	15.01.00	43.50	4.16	1335.00	220	237
weld run 3 - start	15.04.10	46.80		1533.00	210	230
weld run 3 - finish	15.09.00	51.50	4.70	1815.00	250	260
weld run 4 - start						
weld run 4 - finish						
grinding start	15.26.40	1.09.20				
grinding finish	15.45.00	1.27.50	18.30			

Table 1.1 - Time and temperature history of the successful experiment [10]

Unfortunately no clear information is available regarding the exact location of the two points A and B. However, from the sketch shown in Figure 1.10 (from [10]), it could be assumed that they were placed close to the two corners of the cavity.

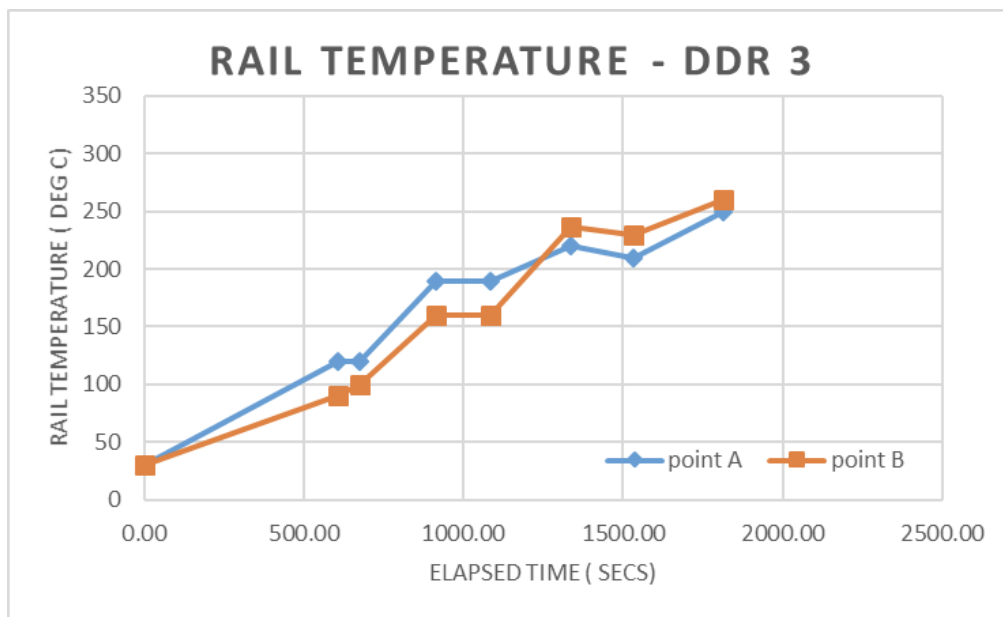


Figure 1.9 - Time-temperature graph for the complete trial in York [10]

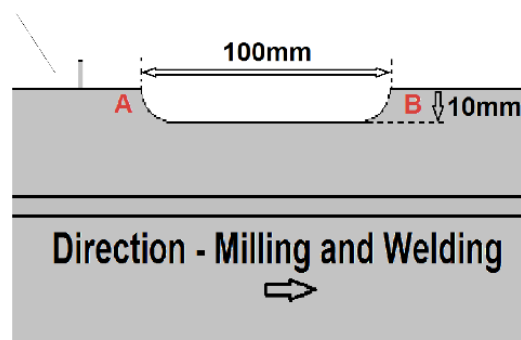


Figure 1.10 - Approximate positions of temperature measurement points A and B [10]

In comparison, Figure 1.11 shows the thermal history for a material point (located exactly at the centre of the cavity in the longitudinal direction and some 7.5 mm in from the gauge face of the rail) in a Flux Cored Arc Welding (FCAW) four-layer experiment carried out by British Steel in May 2008. Note that this graph refers to a different experiment than the one analysed in this Master Thesis. However, since the two repair processes have similarities, the data is still useful in providing a rough picture of the evolution of the thermal fields in the rail and estimate temperatures at which the filler material is deposited in the cavity.

Note the four peaks in Figure 1.11. This is due to the fact that the results refer to a trial in which four layers of welding material were used to fill the cavity. The numerical simulations that will be presented in this report consider three layers in order to match the conditions in the York experiments described above.

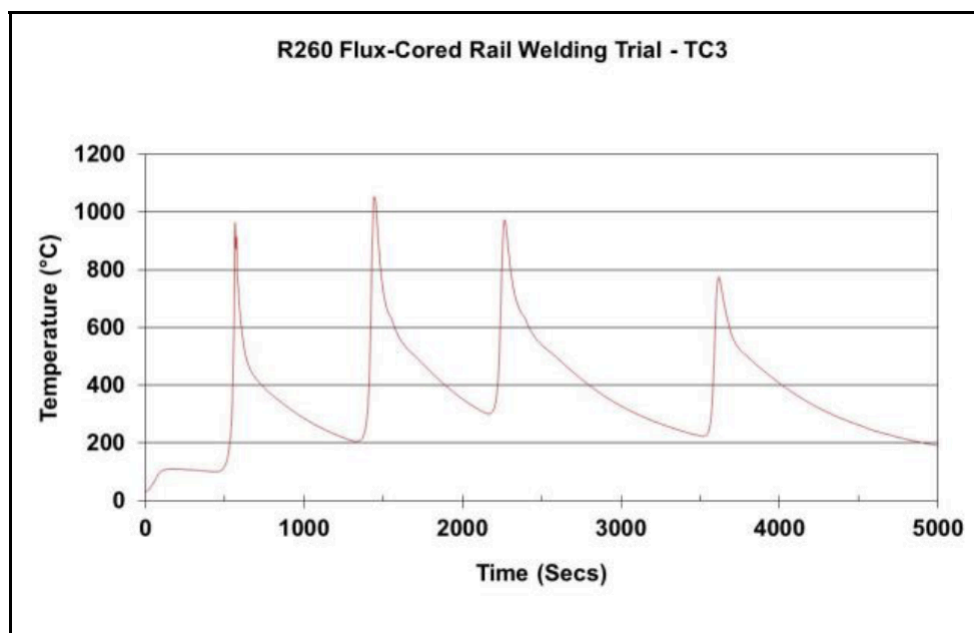


Figure 1.11 - Thermal history for a 4-layer FCAW repair welding experiment [7]

## 2 Scope & aims

The target of this Master Thesis work is to analyse the thermal history to which the rail material is subjected under the British Steel DDR welding procedure. The main aim in performing such analyses is the possibility of predicting the risk of phase transformations that the steel might undergo when the repair welding process is conducted.

It is indeed undesirable to have martensitic areas in a rail head since these tend to be hard and brittle, whereas an austenitic or pearlitic microstructure has more ductile mechanical properties. Knowing the trend of the rail temperature in time and especially in some critical points close to the weld allows contractors and infrastructure managers to identify where welding cracks or phase changes are more likely to occur, see Figure 2.1. This allows for more detailed inspections to identify and mitigate any such cracks.



Figure 2.1 – Fatigue initiation feature in a MMA weld repair of rail [5]

Some experimental data were obtained during the trial held in York in June 2016. These results are listed in section 1.4. To further investigate the temperatures during the trial, a computer model of the whole area affected by the repair procedure was developed. This model is used to predict the detailed temperature distribution throughout the experiment. Unfortunately due to the uncertainties related to the thermocouples position and reliability, it has not been possible to validate/calibrate the simulations in detail. This will be further discussed below.

The aim of the simulations is to find the thermal history of the rail during the whole welding procedure. Different conditions in which the experiments may be performed are analysed. Temperature fringe and history plots were created for each instant of analysis time. Moreover, temperature evolutions are evaluated for selected material points of interest. These include the centre and the corner points of the cavity where the formation of welding cracks is most likely, and possible positions of thermocouples for comparison towards experiments.

The interesting outcome from thermal histories lays in the possibility of extrapolating the cooling rates that different HAZ regions witness during the repair welding procedures. One can analyse these curves in order to assess whether the cooling rates are too high and the formation of martensite is likely or not.

It can be noted that a detailed transient analysis of this extended thermal process may lead to an excessive use of computer memory, very long computational times and, in the worst cases, numerical issues. Given these considerations, it was necessary to find a reasonable compromise between model accuracy and FE mesh density on one hand, and the computational times and memory usage on the other. This was always done by considering the convergence of results between models of increased detail, and also by comparing simulation outputs to experimental results. More details are presented in the next chapters.

### 3 FE-model

This section details the three-dimensional finite element model of the repair welding procedure consisting in the deposition of three welding layers. Most of the analysis is focused on studying temperature trends and cooling rates in the HAZ.

A reference case (in which the cavity has the geometry provided by British Steel) will be described in detail. Other models are then presented by highlighting differences with respect to the reference case.

The FE model was created with the software ABAQUS 6.14-2 [12] and most of the work was performed in the CAE interface. For the simulation of the welding process the ABAQUS Welding Interface (AWI) plug-in (version 2014) developed by Simulia South [13] was used. More details about the numerical simulations are given in the following sections.

Different model configurations were considered. The output of the simulations was compared to the experimental results in order to evaluate robustness and reliability. Moreover, some sensitivity analyses were carried out.

#### 3.1 Geometry

##### 3.1.1 Rail

Rail dimensions are taken from the official definition of the rail profile 60E1 (UIC60) given by Banverket (which is nowadays part of Trafikverket, the Swedish Transport Administration), see Figure 3.1 and [15].

The York experiment was carried out on a 56E1 piece of rail, but the differences in dimensions are negligible from a thermal point of view. This especially relates to the rail head area [15], see Figure 3.1.

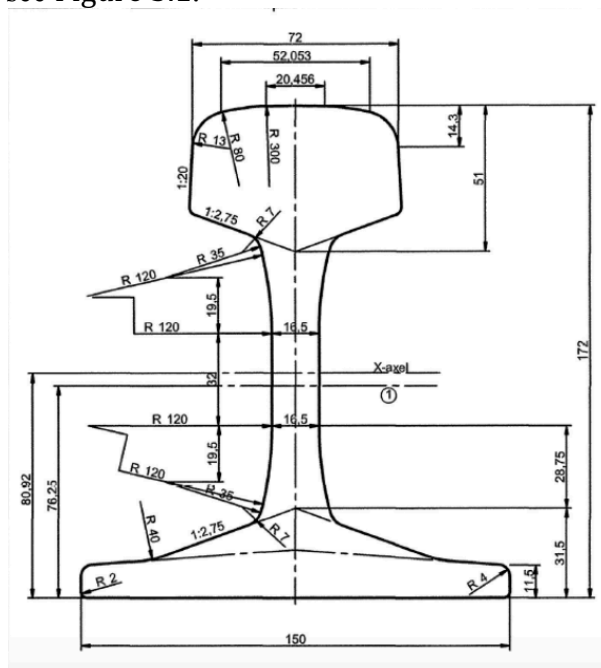
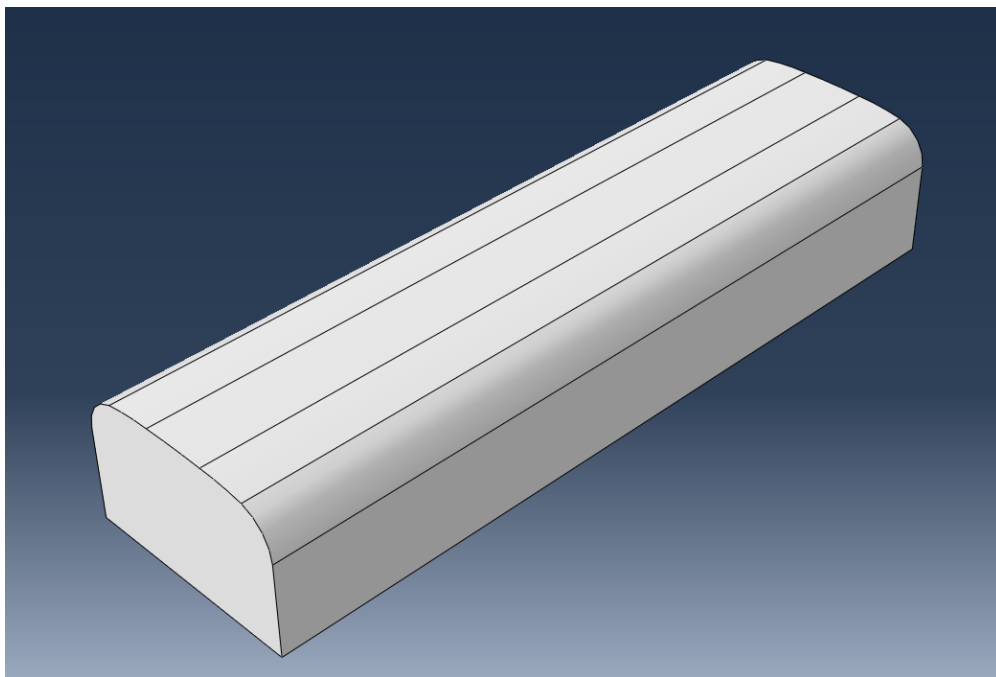


Figure 3.1 – Rail profile 60E1 (also known as UIC60) [15]

In order to keep the complexity of the model within an acceptable level, the rail foot has not been included in the model. Instead, a representative mechanical boundary condition was imposed on the rail head bottom surface. Moreover, the lower part of the head was assumed to be flat (the thermal gradients in this region are negligible with respect to those occurring close to the cavity, so the influence of the simplification is very minor).

The height of the rail head varies between 37.5 and 51 mm (see Figure 3.1). The modelled rail head employed the average height of 44 mm.

Since the model is aimed at simulating the thermal effects on the area surrounding the cavity, one of the problems was deciding the required length of the rail model. The deposition of the filler material warms up the metal below the cavity, but also leads to thermal conduction along the rail. Since the conduction acts as a thermal sink, it is important that the modelled length of the rail is sufficient to capture this effect. On the other hand, modelling a very long piece of rail would lead to significantly heavier simulations. Based on convergence studies, the final model employed length of 250 mm, see Figure 3.2. That means that 75 mm of rail were placed on each side of the 100 mm long cavity.



*Figure 3.2 – Rail model employed in FE-analyses*

### **3.1.2 Cavity**

The shape of the cut-out was one of the main concerns that this Master Thesis work should have examined. The geometrical characteristics of the two corner points can be decisive from the point of view of cooling rates and the formation of welding cracks.

The modelling of the cavity was set out from the drawing in Figure 3.3, which illustrates the standardised dimensions of the cavity for the British Steel experiment [16] where the excavation is 100 mm long and 10 mm deep. It spans throughout the whole width of the rail (about 72 mm). The lateral walls are inclined 45° and transition to the bottom of the cavity is presented by two fillets with a 5 mm radius.

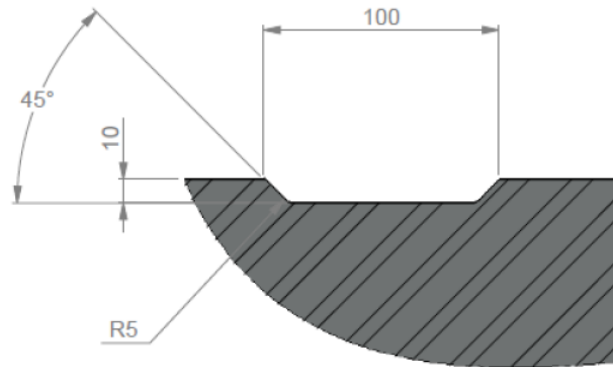


Figure 3.3 – The official geometry for the cut-out, dimensions are in millimetres [16]

However, from pictures taken during the day of the experiment (see e.g. Figure 3.4), it seems that the geometry differs significantly from the one in Figure 3.3. More specific, the corners look a bit sharper, as if the fillet had a radius smaller than 5 mm.



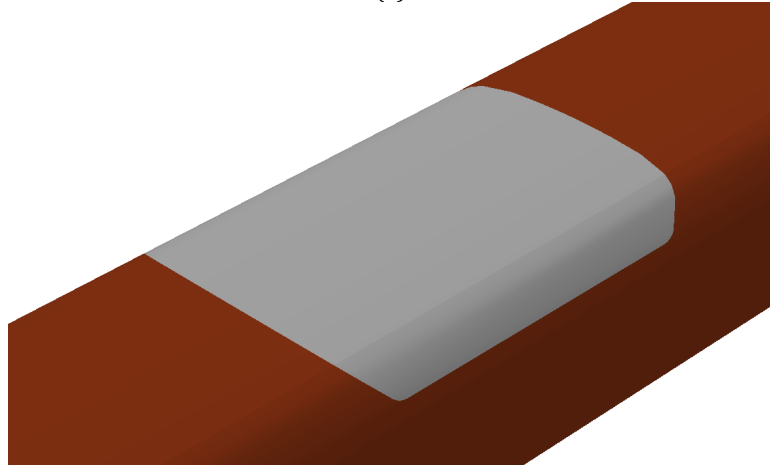
Figure 3.4 – Actual geometry of the cavity during the York experiments in June 2016 (picture courtesy Elena Kabo)

This uncertainty related to the actual dimensions of the cavity initiated the creation of three different models of the geometry of the cavity.

The first (and main) model was characterised by the geometry given in Figure 3.3. This was the geometry with which the main results were derived and further analyses (such as the sensitivity analyses) carried out. A FE-model featuring such a cavity can be seen in Figure 3.5.



(a)



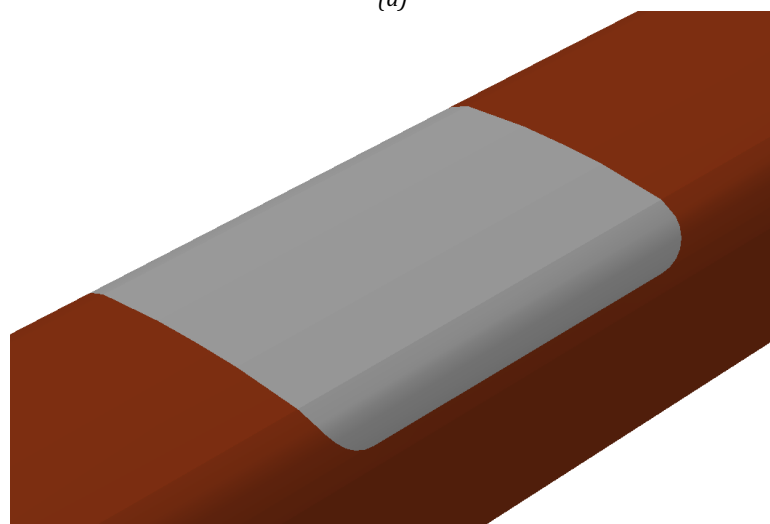
(b)

Figure 3.5 (a) and (b)– FE-model of a rail with a cavity as described in Figure 3.3

Two additional models were created in order to represent two extreme cases regarding the fillet radius: The first model lack inclined walls in the cut out. Instead two rounded fillets with a radius of 10 mm connect the bottom of the cavity to the rail head, see Figure 3.6.



(a)



(b)

Figure 3.6 (a) and (b) – FE-model of a rail featuring a cavity with vertical walls built up with radii of 10 mm

The second case considers the theoretical possibility of having a sharp corner (in which the fillet radius is equal to zero) and lateral walls inclined  $45^\circ$  with respect to the base of the cavity, see Figure 3.7.

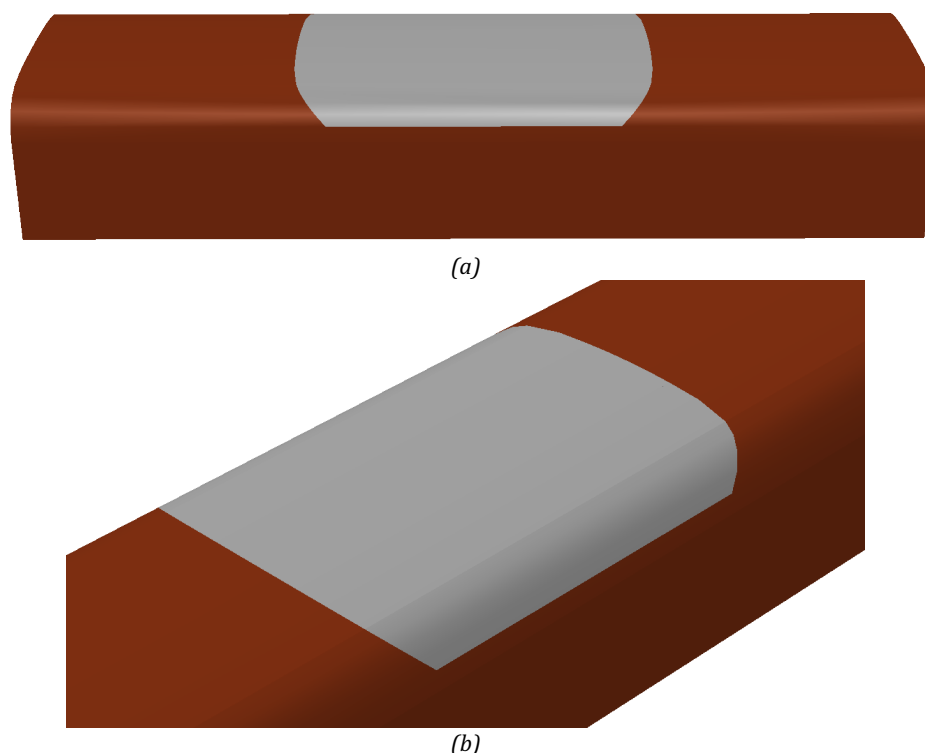


Figure 3.7 (a) and (b) – FE-model of rail with a cavity featuring  $45^\circ$  inclined walls with no transition radius

## 3.2 Boundary conditions

The model is characterised by a multitude of boundary conditions (BC). A small part of these are kept unchanged throughout the whole analysis, whereas the majority of the boundary conditions are activated and deactivated during the different stages of the welding process.

All BC are managed by the AWI plug-in according to instructions given by the user during the definition of the welding process characteristics. Most BC are described in detail in the following sections. In addition, some predefined fields are imposed by the AWI in order to define the initial temperature of the rail and of the filler material.

As for the permanent boundary conditions, it was mentioned in section 3.1.1 that the rail web and foot were not modelled. Instead, they were replaced by a mechanical boundary condition on a strip going through the bottom face of the rail head as seen in Figure 3.8.

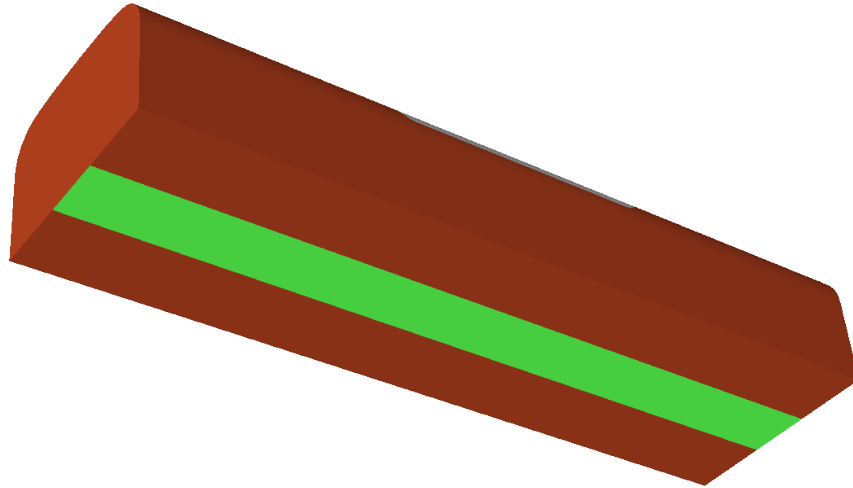


Figure 3.8 – Strip (highlighted in green) where the mechanical BC is applied

Since all analyses carried out for this thesis focused on heat transfer, temperature boundary conditions were extensively used.

First of all, in order to simulate the cooling effect the surrounding track structure has on the temperatures of the repaired area, fixed temperature BC of 20°C (considered as the ambient temperature) were imposed on the right and left vertical end posts of the rail model, see Figure 3.9.

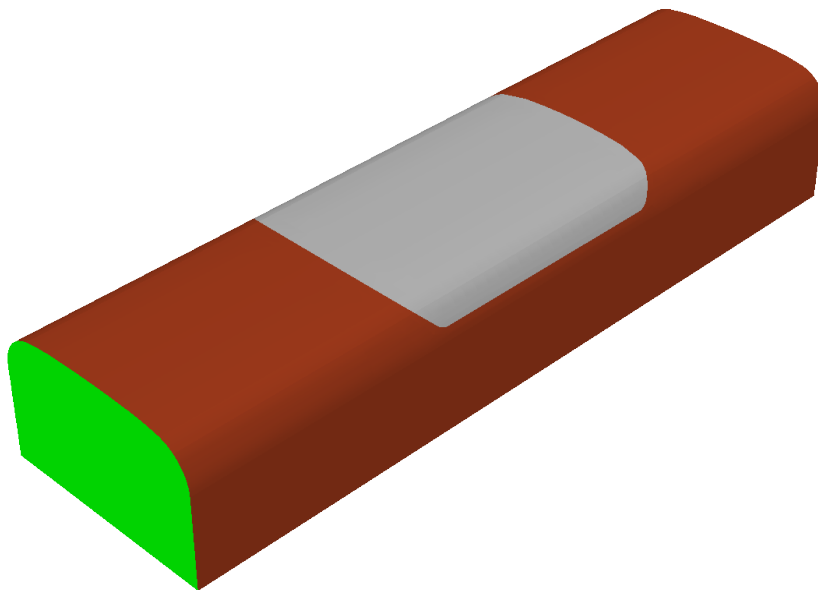


Figure 3.9 – One of the end posts on which the 20°C BC was applied (highlighted in green)

As discussed above, predefined fields were used to describe the initial conditions of the material. In order to simulate the preheating employed in the British Steel welding process, a 80°C field was imposed on the base material of the rail. It is important to consider this temperature since the very low preheat is a distinctive feature of this process as compared to the other methods. Moreover, one objective of the study is to obtain temperature trends in the area affected by the DDR procedure. Here the preheat temperature might have a strong beneficial or negative effect.

Regarding the welding material, no data were provided about the temperature at which it was laid onto the cavity. Some clues came from the temperature trends

registered by the central thermocouple in the 4-layer British Steel experiment shown in Figure 1.11. There it is possible to see that peak temperatures correspond to time instants in which the material is deposited and that the temperatures are always around 1000°C. However, the thermocouples that registered the temperatures were located at a depth of about 2.5 mm from the milled surface [16], therefore the temperature of the molten material must have been higher.

The graph refers to an experiment performed in March 2008 with another type of DDR procedure [7]. The melting temperature for the filler material employed during that experiment was 1510°C and as the material was laid on the cavity in a molten state, its temperature must have been equal or higher than that value [16] [17] (the temperature at which the welding metal is deposited was required by the Welding Interface in order to create appropriate temporary boundary conditions throughout the different analyses). Several temperatures have been employed in the analyses in this thesis. In additions, simulations comparing different filler material temperatures (using the same FE-model) have been performed. The resulting cooling curves have been compared in order to estimate the sensitivity of the analysis, see section 4.3.1.

### 3.3 Material properties

#### 3.3.1 Rail material

The repair welding procedure on which the analyses are focused is meant to be performed on the conventional rail grades R220 and R260. The experiments were carried on a R260 piece of rail. Consequently R260 material data have been employed in the analyses. The main chemical composition of the R260 grade rail steel are presented in Table 3.1. The steel density is 7850 kg/m<sup>3</sup> according to [17].

Element	C	Si	Mn	P	S
wt. %	0.73	0.297	0.998	0.014	0.017

Table 3.1 – Chemical composition of R260 grade rail [17]

Regarding temperature dependent elastic properties, it was recommended by British Steel [17] to use values belonging to BS060A55, a medium carbon steel with a carbon content in the range between 0.3% and 0.5% in weight. The data used in the analyses are listed in Table 3.2.

Temperature [°C]	Young's modulus [GPa]	Poisson's ratio
20	210	0.280
50	209	0.282
100	207.5	0.284
200	202	0.289
400	186.5	0.299
600	165	0.310
650	158	0.314
700	136.5	0.326

Table 3.2 – Temperature dependent elastic properties of the BS060 A 55 medium carbon steel [17]

The thermal conductivity data, which are fundamental for the analyses, were taken from those of a 0.8% C eutectoid steel, see Table 3.3, since they are not expected to vary more than 0.07% with respect to the actual R260 grade ones [17].

Temperature [°C]	0	50	100	200	300	400	500	600	700
Thermal conductivity [W/m/°C]	49.8	49.4	48.1	45.2	41.4	38.1	35.2	32.7	30.1

Table 3.3 – Thermal conductivity for an eutectoid steel [17]

According to the recommendations from British Steel [17], additional thermal properties (specific heat capacity and expansion coefficient) should be similar to those of a medium carbon (0.55%) steel, see Table 3.4.

Temperature [°C]	Specific heat capacity [J/kg/K]	Thermal expansion coefficient [ $10^{-6} \text{ } ^\circ\text{C}^{-1}$ ]
20	430	
50	450	11.35
100	480	11.65
150	505	
200	530	
300	565	
400	610	13.70
500	670	
600	760	14.65
700	710	10.65

Table 3.4 – Specific heat capacity and thermal expansion coefficients for a medium carbon steel [17]

### 3.3.2 Filler material

The filler material comes from a self-shielded flux-cored wire. Its name was “OK Tubrodur 15.43”, but has now been rebranded as “ESAB Tubrodur 35 OM”. It is a common material for basic welding of railway and tram tracks.

According to the ESAB catalogue [18], the chemical composition of the all weld metals are as presented in Table 3.5:

Element	C	Si	Mn	Cr	Ni	Mo	Al
wt. %	0.14	0.3	1.1	1.0	2.2	0.5	1.5

Table 3.5 – Chemical composition for OK Tubrodur 15.43 [14]

The information in the catalogue was not focused on the thermo-mechanical properties which are important in heat transfer analyses. However, as stated in [19], the thermal characteristics of ESAB Tubrodur 35 OM are approximately similar to those of a low carbon steel. Consequently, data for a steel containing between 0.15% and 0.23% of carbon were used [17], these data are presented in Table 3.6 to Table 3.8. A typical density for steels ( $7800 \text{ kg/m}^3$ ) was presumed.

Temperature [°C]	Young's modulus [GPa]	Poisson's ratio
20	212.4	0.288
100	208.9	0.290
200	201.3	0.293
400	184.1	0.300
600	166.2	0.306
650	157.2	0.311

Table 3.6 – Elastic properties for a 0.15 % carbon steel [17]

Temperature [°C]	20	50	100	200	300	400	500	600	700
Thermal Conductivity [W/m/°C]	52.0	51.7	51.0	48.8	46.0	42.7	39.2	35.2	26.5

Table 3.7 – Thermal conductivity for a structural 0.20% carbon steel [17]

Temperature [°C]	Specific Heat Capacity [J/kg/K]	Thermal Expansion coefficient [ $10^{-6} \text{ } ^\circ\text{C}^{-1}$ ]
20	440	
50	450	11.92
100	480	12.18
150	505	
200	530	
300	565	
400	610	13.47
500	675	
600	800	14.41
700	1340	14.88

Table 3.8 - Thermal properties for a structural 0.20% carbon steel [17]

### 3.4 Discretisation

#### 3.4.1 Weld beads

For the reasons described in section 3.3.2, three different geometries for the cavity were created. In all cases, the cavities were not modelled in ABAQUS/CAE as a separate part, but as a partition of the rail. The two materials (R260 grade and OK Tubrodur 15.43) were defined in the model with material properties given in section 3.3.

As for the different weld beads, they were modelled by means of rectangular chunks. Since the cavity was 10 mm deep and was fully covered with three layers as in the trials in York [10], the first two layers were partitioned in order to be 3 mm thick and the last layer featured a (maximum) height of 4 mm, see Figure 3.10. The depth was measured from the highest point of the rail head, as a consequence of the rounded rail head, the average thickness was therefore lower than 4 mm.

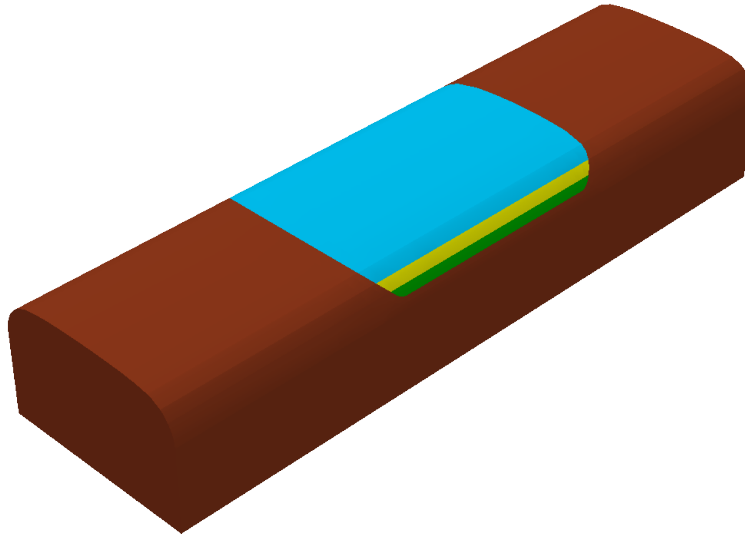


Figure 3.10 – The three welding layers represented in the main model

Another problem was estimating how many beads (i.e. welding segments) were used in the trial held in York in order to complete a layer. No exact information was provided from the experiments. A realistic estimation was made based on Figure 1.7 and other similar pictures taken during that day. The conclusion was that around 20 to 22 passes were needed to cover the surface of the cavity. For this reason the bottom layer was split in 20 parts by means of appropriate partitions in ABAQUS/CAE, see Figure 3.11.

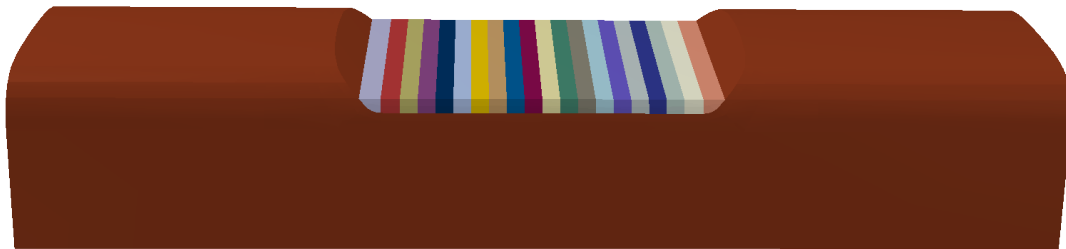


Figure 3.11 – The different weld beads represented on the first layer of the main model

As can be noticed in Figure 3.5 to Figure 3.7, the surface covered by the welding layers increases as they get more distant from the bottom of the cavity. In order to keep the volume of filler material laid by each pass somehow constant, the two upper layers were modelled with 22 beads. This was useful also to take into account the longer time needed to complete the last layers, see Table 1.1.

As seen in Figure 1.7 and described in section 1.3, the final rail geometry cannot be reached by just filling the cavity with the welding material. Some slag has to be removed after each pass and the welding nozzle has to be carried back to its original position. Those operations took on average 3 minutes per pass, see Table 1.1, and allowed the repaired area to cool down. As a consequence, some intercooling steps of 180 seconds each were introduced in the simulation model after the completion of each welding layer. In addition, some material in excess is expected to be found on both the weld sides and the top, and that has to be taken away at the end of the process by means of grinding.

However, the final grinding phase (like the milling at the beginning of the process) has no significant effect on the thermal history, nor on the metallurgical transformation of the material. Therefore it will not be considered throughout the following numerical analyses. As a consequence, the computer model of the welding process will just assume that the exact geometry is reached directly after the three welding passes.

### 3.4.2 Finite element mesh

The fact that the different weld beads were modelled as partitions in ABAQUS/CAE was primarily due to the requirements set by the AWI. Some more complex partitions, were introduced in the areas of the cavity corners and close to the rail head radii (where the elements tend to be very distorted, see Figure 3.12).

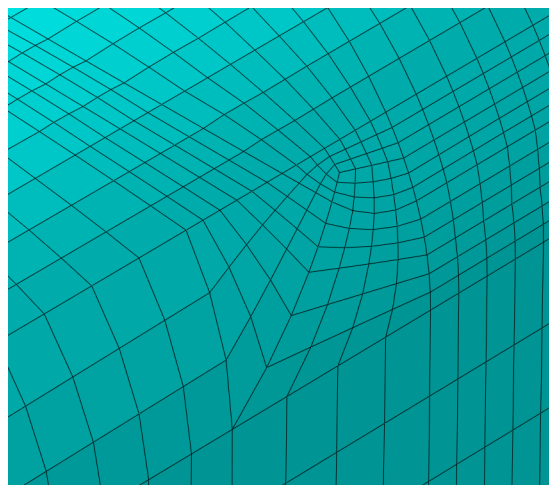


Figure 3.12 – An example of a critical area for meshing: the corner of the cut-out in the main model

Moreover, some vertical partitions were extended up to the base of the rail to keep the element shape as uniform as possible and to split the weld beads in smaller sections called chunks. This allowed improved simulations of the moving source of heat and the gradual addition of material.

The model was partitioned in such a way that the entire cut-out volume could be meshed by using either a structured or a swept mesh. A structured mesh is generated by Abaqus by adapting the mesh of regular and simple regions (such as squares, triangles, etc....) onto the complex geometries of the models. A sweeping mesh is instead defined by creating a 2D mesh on a source side according to the instructions given by the user (e.g. element size, number of elements on specific areas, bias ratio, etc.) and copying these mesh nodes onto a series of layers until the mesh reaches the target side.

In order to use the AWI a swept mesh was necessary in the area filled by the welding material. The reason is that when the plug-in defines the different weld passes the paths of these are identified by using that the mesh is swept along the welding direction. For this reason, a swept mesh was used in the welded area. For the rest of the model (i.e. for the base material) a structured mesh was used.

Regarding the type of elements, heat transfer elements of DC3D8 type were chosen. These are 8-noded linear heat transfer bricks which belong to the ABAQUS' standard element library. They have the nodal temperature as their degree of freedom.

The main criteria for a good mesh were employed here:

- A finer mesh in areas of analytical interest and in the expected zones of stress concentration (or, in this case high temperature gradients). For the current analysis, this implied the cavity corners and the welded area.
- Low element distortion with aspect ratios below 5, element corner angles between 45° and 135°.

These characteristics were pursued by applying appropriate bias ratios on critical areas and by seeding the most important edges.

A vital aspect of the meshing process is the sensitivity analysis. It is well known that if the mesh is too coarse or the elements are too skewed then FE simulations may result in significant errors. The robustness of the output and the reliability of the mesh can be evaluated by comparing simulation results with the experimental ones and/or by performing a convergence analysis with gradually refined meshes. When the results of two consecutive meshes (essentially) converge, the coarser mesh is sufficient for the analysis.

A sensitivity analysis was carried out in the study. Details and output are presented in section 4.1.

### **3.5 Modelling of the welding process**

The modelling of the thermal history of a welding process in ABAQUS/CAE requires the definition of many steps, introduction of boundary conditions with subsequent deactivation (and reactivation) of the different partitions in order to simulate the gradual addition of the welding material. This approach can get very time consuming, especially if the model is characterised by a large number of welding beads, such as in the current study.

In order to reduce computational times for repetitive actions (e.g. activating and reactivating temporary BCs, defining the surfaces on which conduction and radiation act on each step, etc.) the ABAQUS Welding Interface (AWI) plug-in can be employed. The AWI has been discussed in the previous sections of this report, but it will now be described in detail.

#### **3.5.1 Weld definition**

Once the model has been created, materials have been defined and the full geometry was meshed, the AWI could be employed for the welding process definition. First of all, it was necessary to define welding order and path. Since the interface expects weld passes to be straight, a swept mesh was required in the weld area (as discussed above).

Three different welds were defined (one for each layer) and the beads were chosen according to the welding order used to fill the cavity with a zig-zag path which moved from one wall of the cavity to the opposite one. Once the beads were defined, the interface automatically created chunks according to the vertical partitions of the rail.

The interface then used chunks in order to split each bead in smaller parts. The gradual addition of filler material can thus be discretised by a sequential activation of these small volumes.

### 3.5.2 Pass and job definition

The AWI required information on the single passes and on the characteristics of the analyses. With the term “pass”, the interface considers a part of a weld bead that is activated in a single step during the analysis process.

As a consequence, the definition of a very high number of passes for each bead makes the analysis very close to the reality, i.e. to the gradual addition of the filler material. On the other hand, every time a pass is defined, the interface has to create a large number of steps, interactions, temporary boundary conditions, etc. Thus, the analysis gets extensive and slow. A trade-off analysis was made where it was found to be appropriate to define three passes for each weld bead, i.e. between 60 and 66 passes for each layer, see Figure 3.13. This can be compared to the fact that the interface tends to crash during the job definition phase if the number of passes goes above some 300–400.

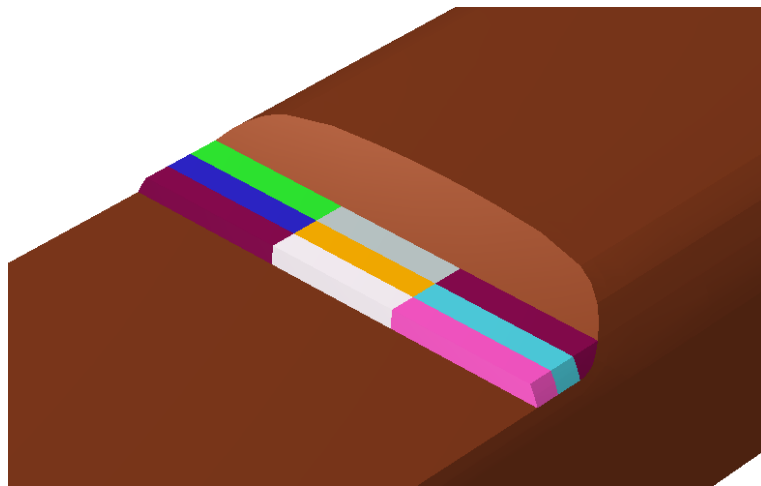


Figure 3.13 – Colour-coded representation of the division in passes of the first three weld beads

At this point, the interface requests information regarding the timing of the process. In order to keep the welding time around 4 minutes (or slightly above for the last layers, according to the trials in York [10]), each pass was set to have a time period of 4 seconds. This period was split in several time increments by the analysis software according to the temperature variation trend.

### 3.5.3 Temporary boundary conditions

After the different passes were defined, the AWI was provided with some data on the thermal characteristics of the process.

First of all, as discussed in the previous section, the temperature at which the molten welding metal is laid was requested. The technical staff from British Steel [16] estimated that temperature to be above 1510 °C, but the comparison between the numerical results and the thermal histories recorded during some trials [16] suggested that the filler material temperature could be as high as 1700 °C, see section 4.3.1.

The given values were used by the AWI to apply temporary temperature boundary conditions on the surfaces on which the filler was deposited, and for the amount of time that was required in order to complete each single pass (4 seconds in all the analyses described in this report). After that, the software activated the quantity of material corresponding to the filler deposit during the pass. The filler was applied at the requested predefined temperature according to what was specified in the interface settings. In the following step, the interface applied the same BCs on the areas affected by the subsequent pass, while the material belonging to the previous step was allowed to cool down.

Data regarding the metal-to-air convection were also needed. Unfortunately no precise information has been provided regarding this property for the R260 rail steel and for ESAB Tubrodur 35 OM. Instead, a reasonable value for steels was used (25 J/s/m<sup>2</sup>/K) [13]. The convection interaction was applied on the whole free surface of the rail (apart from the bottom surface and the end posts, where an ambient temperature condition was imposed). Moreover, the plug-in created some small surfaces corresponding to the faces of the cavity and of the weld beads on which the convection interaction could be activated and deactivated. That depended on whether those areas were in contact with air or not during a certain stage of the repair process.

### 3.5.4 Intercooling steps

As mentioned in the description of the process, some time was spent in between the deposition of the different layers in order to remove the slag and to prepare the procedures needed for the completion of the next welding phase. Although, according to [10], the time required to carry this operation was not fixed, it was possible to notice that it was around 3 minutes (Table 1.1). During that time frame, the rail was allowed to cool down, which had an effect on temperature and, subsequently, on the thermal behaviour during the deposition of the following layer.

For the sake of precision and realism, three “cooling steps” of 180 seconds were defined after each welding phase in the simulations. To make the cooling process more realistic, these steps were characterised by the same boundary conditions and interactions which were active at the moment in which the last welding pass was laid. A final cooling step of 180 seconds was defined after the end of the whole filling process (i.e. at the end of the deposition of the third layer) in order to be able to predict the cooling characteristics of the whole repaired area after the completion of the welding procedure.

### 3.5.5 Thermal fluxes

Two different types of thermal fluxes were taken into account: thermal conduction within the material, and the convection between the air surrounding the rail and the filler material.

Regarding thermal conduction, its magnitude is mainly dependent on the thermal gradient and the conduction coefficient, see equation (1) [12].

$$q_c = -k \cdot \nabla\theta \quad (1)$$

Here  $q_c(x, t)$  is the heat flux density [ $\text{W}/\text{m}^2$ ],  $k(\theta)$  the material conduction coefficient [ $\text{W}/\text{m}/^\circ\text{C}$ ] (which depends on whether the heat flux is computed within the rail or the filler material and on the current temperature, as detailed in section 3.3),  $\theta(x, t)$  [ $^\circ\text{C}$ ] is the temperature at a certain material point at a certain time.

According to the numerical results, thermal conduction was the main form of heat exchange within the model. However, convection between the rail material and the surrounding air has been fully considered in the analyses. Convection,  $q_s$ , can be estimated from

$$q_s = -\mathbf{n} \cdot h \cdot \nabla\theta \quad (2)$$

This is the boundary term of the general convection law [12]. Here,  $h$  is the steel-to-air convection coefficient, whose average value is 25 [ $\text{W}/\text{m}^2/^\circ\text{C}$ ] [13] and  $\mathbf{n}$  represents the normal vector of the surface which is affected by convection.

## 4 Results

### 4.1 Sensitivity analysis

As discussed in section 3.4.2, a sensitivity analysis was performed in order to evaluate the robustness of the mesh and of the whole modelling of the process. It was considered sufficient to perform these checks only on the reference model (with the cavity geometry defined by British Steel). All other models were then meshed using similar meshes to the sufficiently fine mesh identified by the sensitivity analyses.

Three different meshes were created for the model with the reference geometry. The “coarse” mesh was characterised by elements with a maximum size of 5 mm. In the most important areas (i.e. the corners of the cavity and the rounded surfaces at the sides of the third layer), the element edge was 0.51 mm. The “medium” mesh featured a maximum element size of 3.5 mm and an edge size of 0.35 mm in the vicinity of the corners. The “fine” mesh was characterised by a maximum element size of 2.5 mm which progressively decreased to 0.25 mm near the cavity. The mesh characteristics are summarised in Table 4.1.

Mesh type	Number of DOF in the whole model	Coarsest element size [mm]	Element size close to the corners [mm]
Coarse	29667	5	0.51
Medium	110259	3.5	0.35
Fine	160977	2.5	0.25

Table 4.1 – Characteristics of the three evaluated meshes

Figure 4.1 and Figure 4.2 show the differences between the three meshes in the corner areas

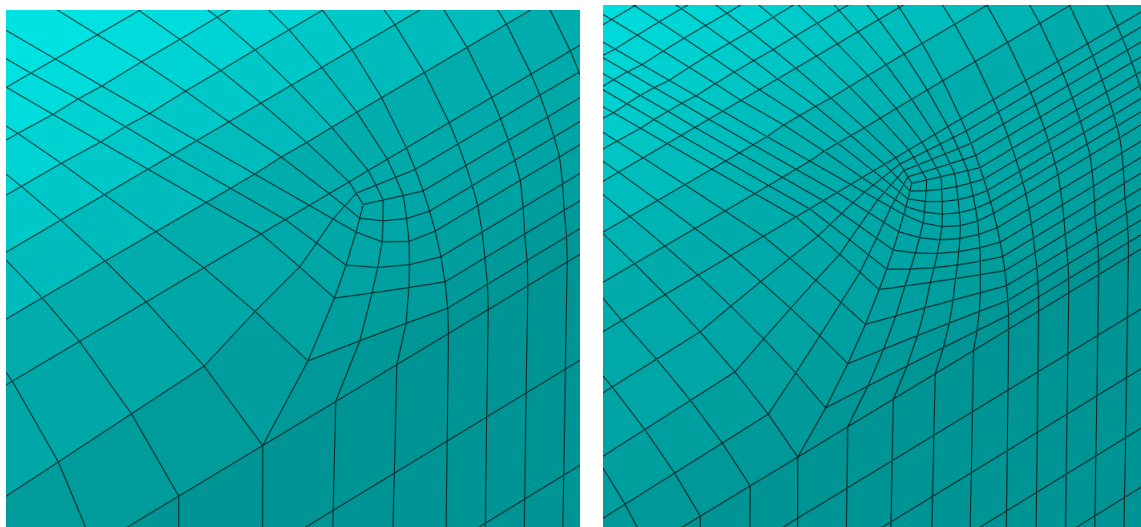
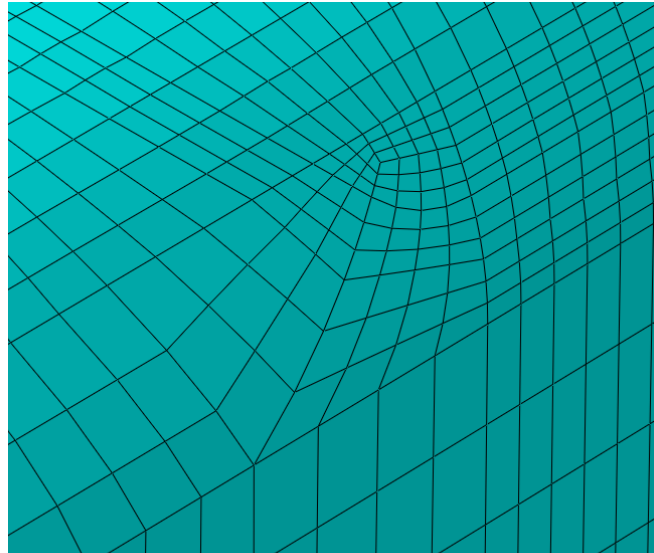
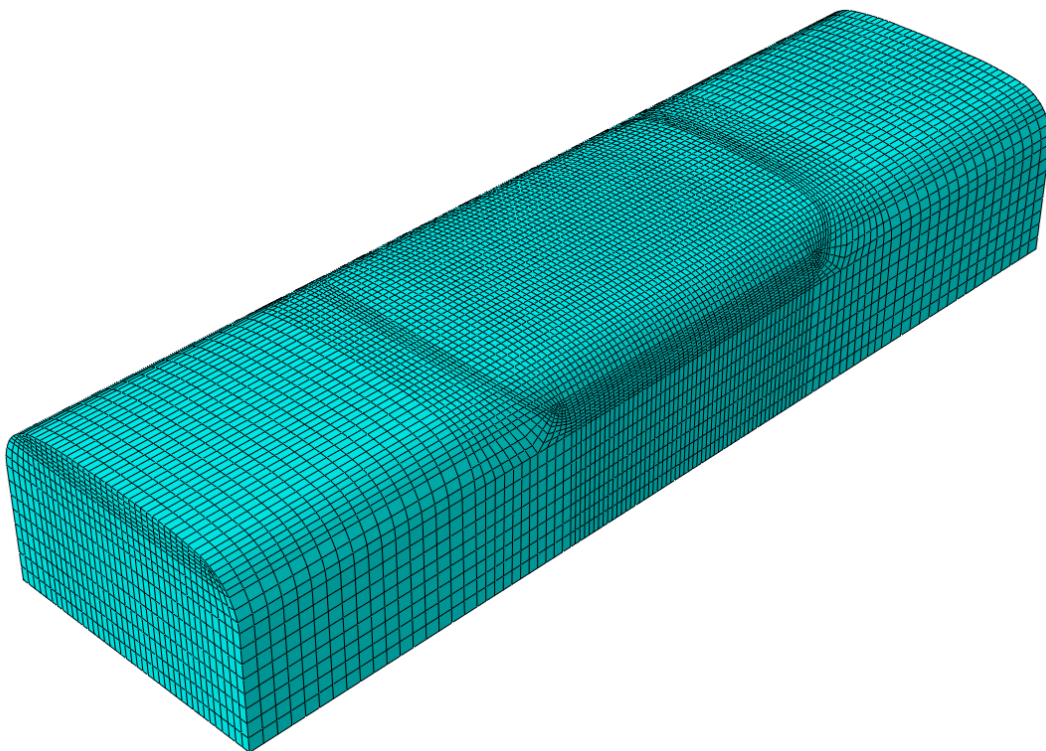


Figure 4.1 – The cavity corner with the “coarse” mesh (left) and the “fine” mesh (right)



*Figure 4.2 - Mesh of the cavity in the adopted ("medium") model*

The way the whole rail head was meshed in the final model using the “medium” mesh is shown in Figure 4.3. It is possible to see that the areas with the finest mesh are the areas in the vicinity of the corners, the rounded surfaces and the border areas between the filled cavity and the base material.



*Figure 4.3 - Completed mesh of the "final" model*

After applying the same steps, temperature fields, boundary conditions, etc. three different analyses were run on the three models. The results were compared in order to check the mesh convergence. To make this report more synthetic and easier to read, only some results are presented in this section. Remaining results are presented in Appendix A.

## 4.2 Robustness analysis

Three points in FE-models were chosen for the sensitivity analyses. These were located in some of the most interesting parts of the models, i.e. close to corners, close to the inclined walls and at the centre of the cavity, where the cooling effect due to convection is minimal.

The first point, here referred to as “SA-L” (which stands for “sensitivity analysis – left”) was located close to the corner where the welding process started, exactly 2.4 mm from the cavity, see Figure 4.4. The sensitivity analysis focused not on the full thermal history, but data from significant instants in time. For this reason, only temperature peaks and minima in this point are compared for the three meshes. Evaluated temperatures are presented in Table 4.2:

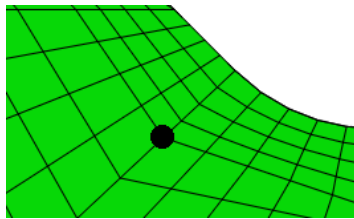


Figure 4.4 – The location of SA-L

Moment	Time instant [s]	Temperatures [°C] and mesh			coarse-medium difference [%]	medium-fine difference [%]
		coarse	medium	fine		
1st peak	8,4	567,7	562,2	561,1	0,97	0,20
1st minimum	421	161,3	157,9	156,6	2,11	0,82
2nd peak	429	479,3	473,9	474,2	1,13	0,06
2nd minimum	865	184,3	179,4	178,2	2,66	0,67
3rd peak	887	442,9	432,5	431,4	2,35	0,25
3rd minimum	1308	194,6	189	188,1	2,88	0,48

Table 4.2 – Temperature values for the FE-node SA-L for the three different meshes

It may be noticed that the difference in results between the meshes designated “coarse” and “medium” is around 2%. That value can already be considered acceptable, but since the element shapes for these meshes were slightly distorted in the areas close to the corners, a third “fine” mesh was prepared. Differences between this “fine” and the “medium” meshes at crucial points ranged between 0,06 and 0,82 per cent. At this point, it was clear that the “medium” mesh was reliable and robust enough to perform thermal analyses with.

It is worth mentioning that for the sensitivity analysis, a standard load case (e.g. employing a predefined temperature of 1150 °C) was used for the filler material. Since the robustness tests had given such a reliable output, it was not considered necessary to perform them again for every change in the analysis procedures.

The full thermal history of the SA-L node according to the medium mesh can be seen in Figure 4.5:

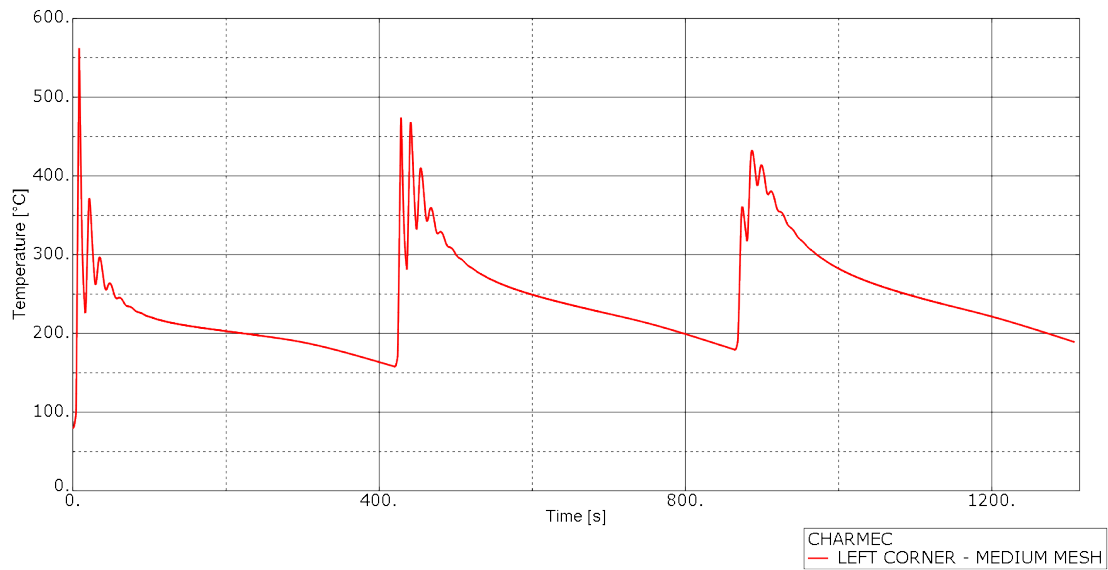


Figure 4.5 – Thermal history for the SA-L node in the final mesh

A comparison of the full thermal history of the point SA-L for all three meshes are presented in Figure 4.6 as the second layer is applied, and in Figure 4.7 as the third welding layer is deposited in the vicinity of the SA-L test node.

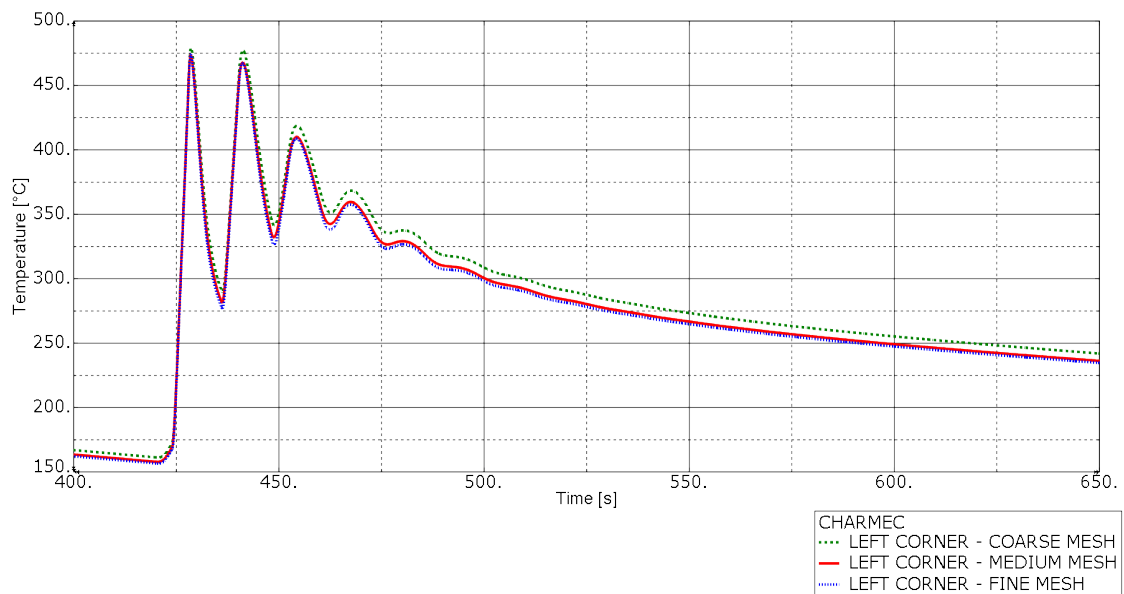


Figure 4.6 – Comparison of the time histories evaluated using the three meshes in point SA-L at instances in time associated to the second layer

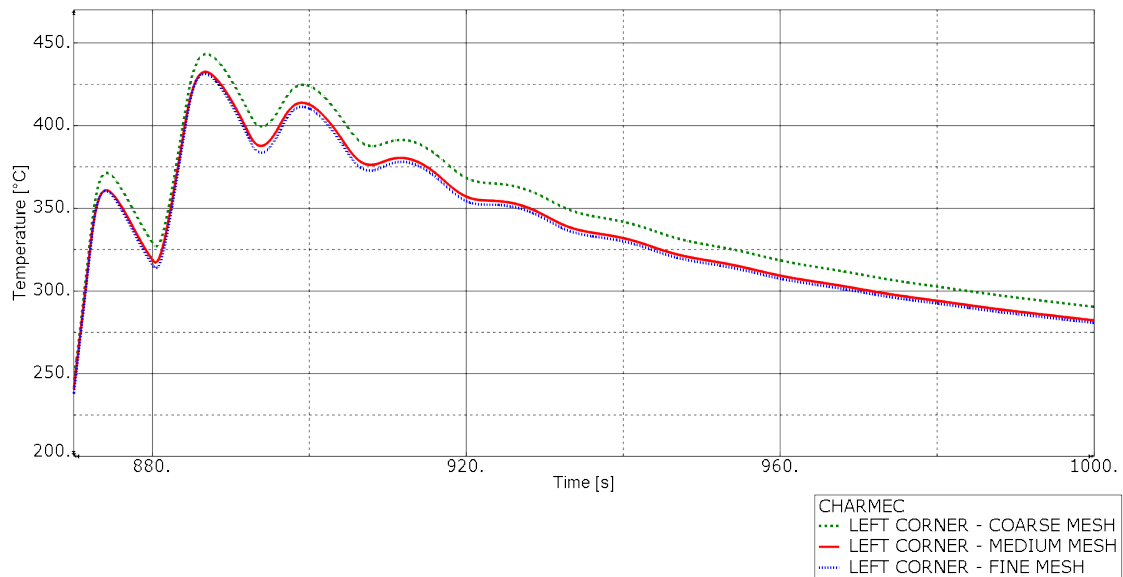


Figure 4.7 - Comparison of the time histories evaluated using the three meshes for the point SA-L for instances in time associated to the third layer

It can be easily noticed that the differences between the three meshes are only visible if the figures are zoomed in. In particular, the discrepancies between the "medium" mesh and the "fine" mesh are negligible.

Similar considerations were made for the other two test nodes. Results for these studies can be found in Appendix A.

### 4.3 Thermal history results

Different types of thermal history plots were produced during the analysis phase and results were compared with those of a similar experiment that was carried out on the same cut-out geometry by British Steel in 2008. That experiment, however, took a different amount of time with respect to the one simulated and analysed in the present study (according to the experiment in York in June 2016 [10]) and consisted of four welding passes [7].

The importance of the trials held in 2008 relates to the fact that five thermocouples were mounted in different points of the base rail material. In the experiment held in York in June 2016 no thermocouples were used and, as a consequence, there was no thermal data on which to calibrate the simulations and/or to validate the numerical results [10].

Figure 4.8 shows the position of the five thermocouples during the trials in 2008. The welding square weave path, in that case, started on the left-hand side of the picture (on the side corresponding to the thermocouple TC1) and proceeded towards the right (as in Figure 4.8), where the thermocouple TC5 was placed. In order to make the simulation results easier to compare, the same numbering order that was used for the thermocouples in the 2008 experiment was kept for the analysed nodes in the FE-models.

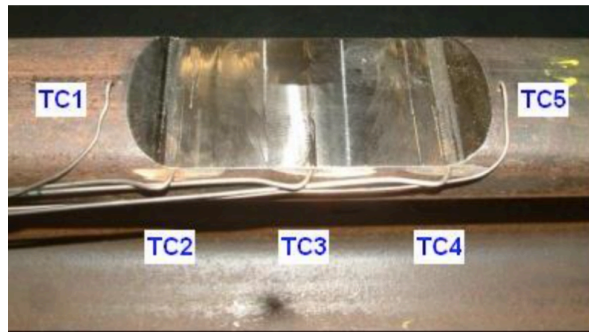


Figure 4.8 – Position of the five thermocouples for the experiment held in 2008 [7]

Two of the five thermocouples (TC1 and TC4) failed during the trial [16], but the other ones were still able to record the full thermal history in their respective locations. The positions of the thermocouples [16] can be seen in Figure 4.9, although it is important to consider that the actual locations might be slightly different due to uncertainties e.g. in hole drilling.

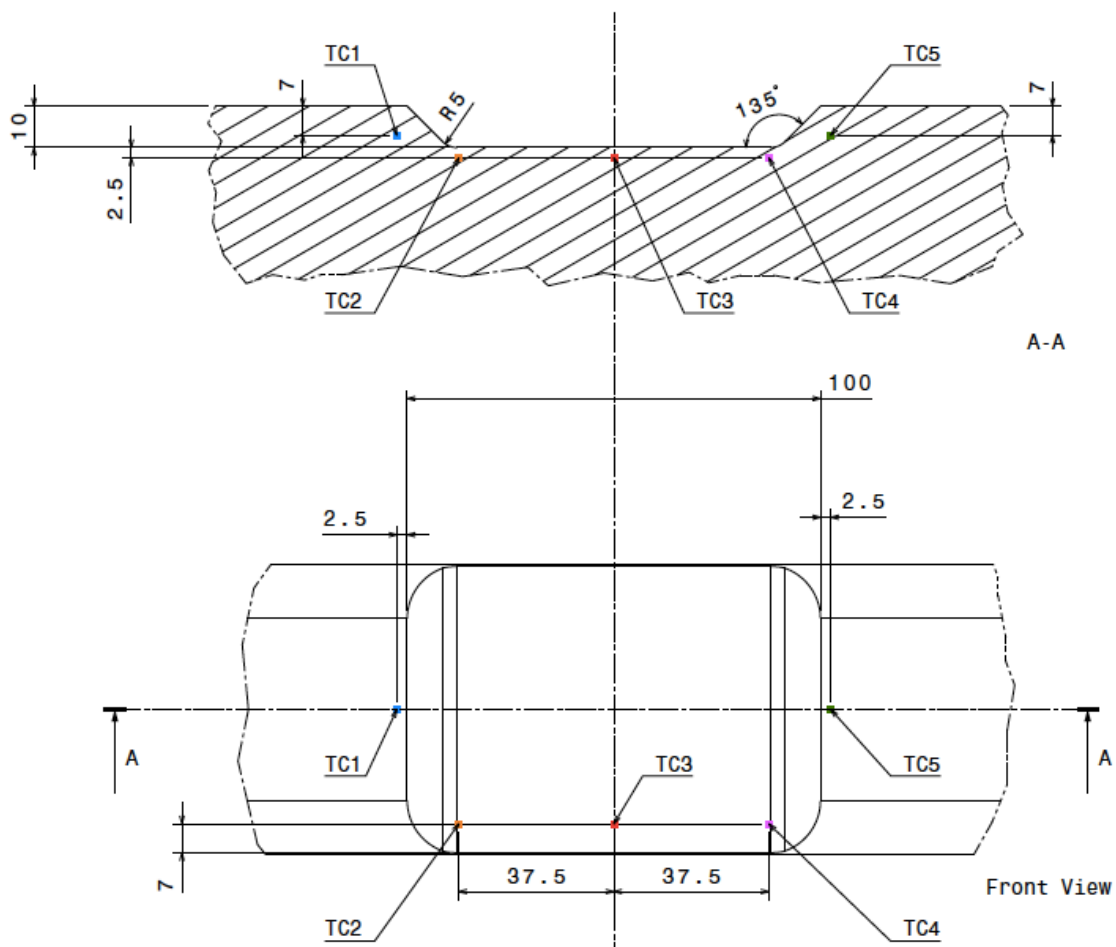


Figure 4.9 – Estimated positions of thermocouples during the experiments in 2008 [16]

### 4.3.1 Influence of the filler material temperature

The first analyses were aimed at studying the temperatures and the cooling rates in the areas corresponding to the thermocouple positions. Most of the attention was put in studying the effect that the temperature at which the filler material is deposited in the cavity has on the thermal history of the HAZ.

Two different temperatures were investigated for the welding material: 1700 °C and 1800 °C. These gave numerical results from the simulations which were closer to those actually obtained in the 2008 experiment [7].

In this section, just the results for the TC3 (the central thermocouple) and TC5 (the one located on the side of the cavity where the welding process terminates) will be compared. The results from the other TCs are not presented in the present report.

Before proceeding with results, more information about the analysis points will be provided: the node which approximated TC3 was located 3.1 mm below the cut-out, at a depth of 8.3 mm from the rail gauge surface, see Figure 4.10 (a value between 5 and 10 mm is generally used in this case in order to avoid the effect of the thermal convection between the rail surface and the surrounding air [16]).

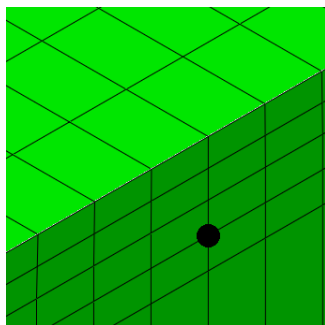


Figure 4.10 – Position of the node used to simulate TC3

The node used to approximate TC5 was located on the rail head centre line, at a depth of 10 mm from the running surface and at a lateral distance of 3.1 mm from the lateral side of the cavity, see Figure 4.11.

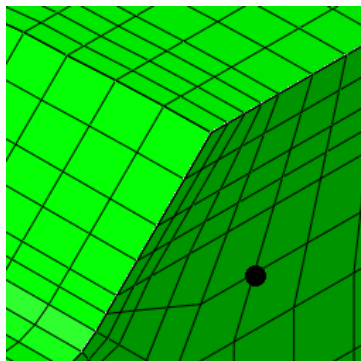


Figure 4.11 - Position of the node used to simulate TC5

At this stage of the analysis the attention was put on the dependency on the filler material temperature. The dependency on the exact location of the point of temperature evaluation (and therefore on the thermocouple position) will be studied in the next section.

Figure 4.12 shows the thermal history that TC3 recorded during the experiment in 2008. Figure 4.13 shows the thermal histories that were obtained in the FE analyses for the different filler material temperatures.

It is worth observing that the preheating phase (which is represented by the initial 400 seconds in Figure 4.12) is not included in the graphs describing the numerical results. That was due to the fact that preheating took 600 seconds, while the rest of the

process was about 1300 seconds long [10]. As a consequence, introducing such long extra time slots would have made graphs more difficult to read. Moreover, heating up the rail from the environment temperature to 80 °C does not have a significant impact on the thermal behaviour of the material, therefore it was not included in the simulations.

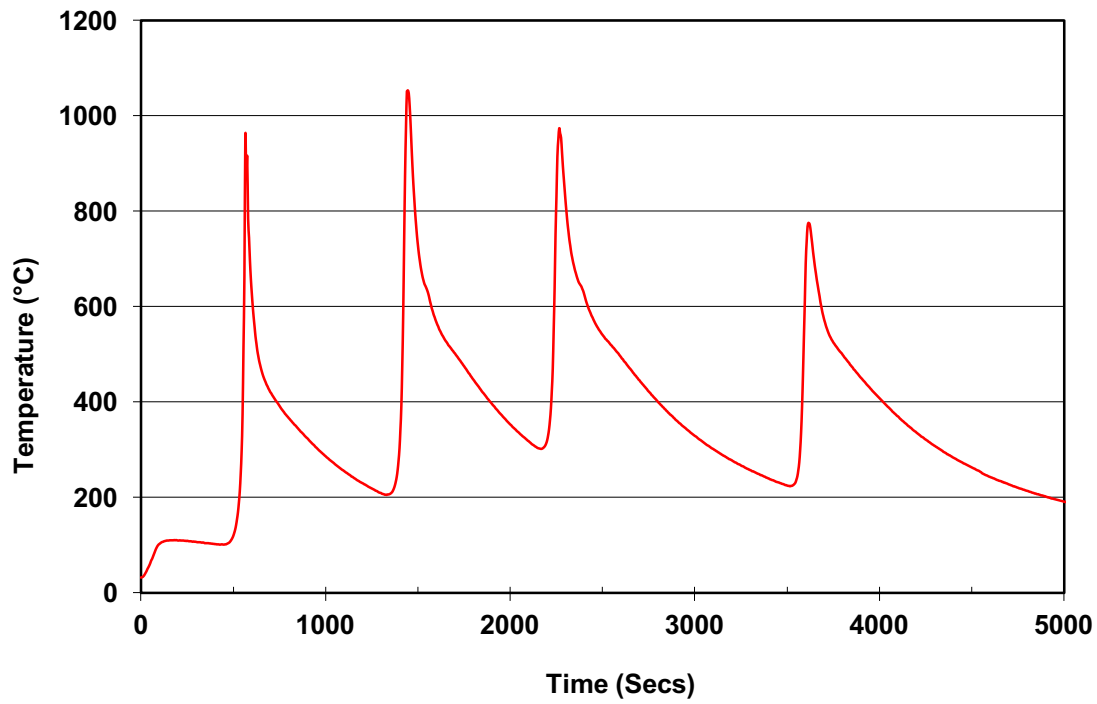


Figure 4.12 – Thermal history of TC3 for the experiment in 2008 [7]

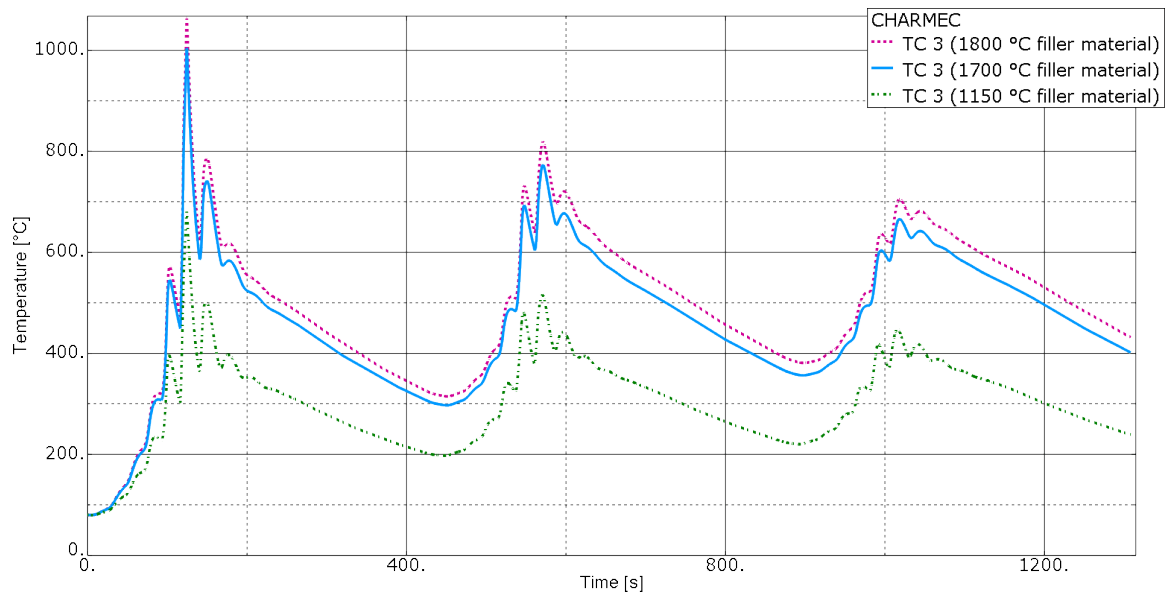


Figure 4.13 – Predicted thermal history for TC3 using different filler material temperatures

It can be seen in Figure 4.12 and Figure 4.13 that the temperature curves are shifted to higher values by the increase in temperature of the filler material.

Similarly, Figure 4.14 is a representation of the thermal evolution obtained by TC5 for the trial in 2008. Figure 4.15 shows predicted thermal histories for TC5 from FE

analyses featuring three different filler material temperatures and gives the same trends as noted from Figure 4.13.

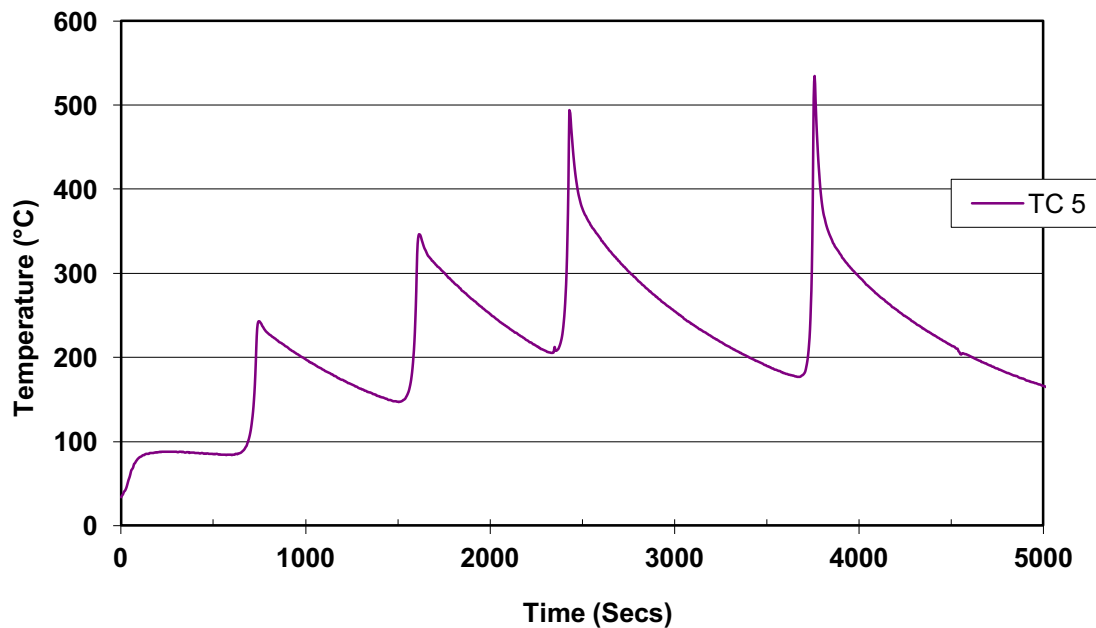


Figure 4.14 - Thermal history of TC5 from the experiment in 2008 [7]

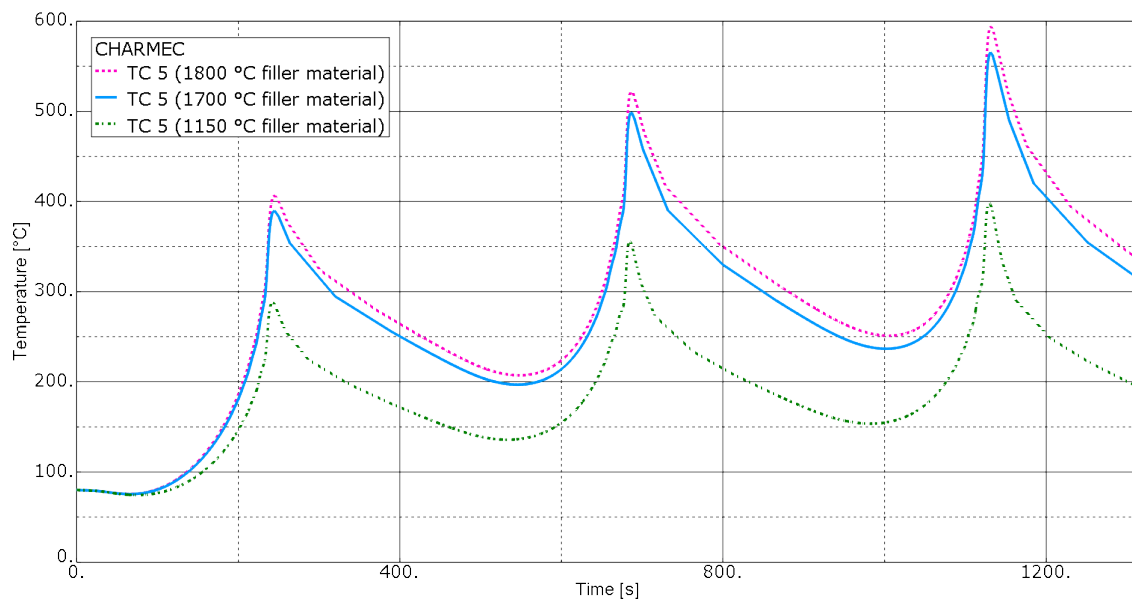


Figure 4.15 - Predicted thermal history for TC5 for different filler material temperatures

### 4.3.2 Influence of the thermocouple position

The second step of the analysis procedure consisted in studying the influence on the cooling curve of the position of the thermocouple. As a consequence, temperature evolutions for some different positions in the vicinity of the estimated thermocouple positions in the 2008 experiment have been derived.

In this analysis, the filler material was kept constant at 1700 °C (selected since it was the temperature which led to the closest results with respect to those obtained in the experiments of 2008, see section 4.3.1).

The three studied positions were all exactly in the middle of the cavity, at a depth of 8 mm from the rail gauge surface. The vertical distances from the cavity were 2.03 mm, 2.79 mm and 3.54 mm, see Figure 4.16.

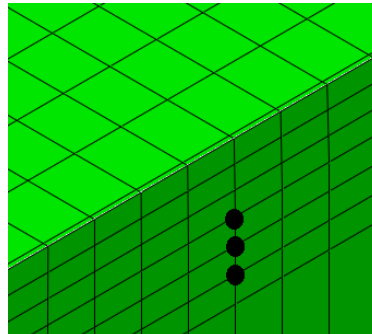


Figure 4.16 – The three analysed locations in the vicinity of TC3

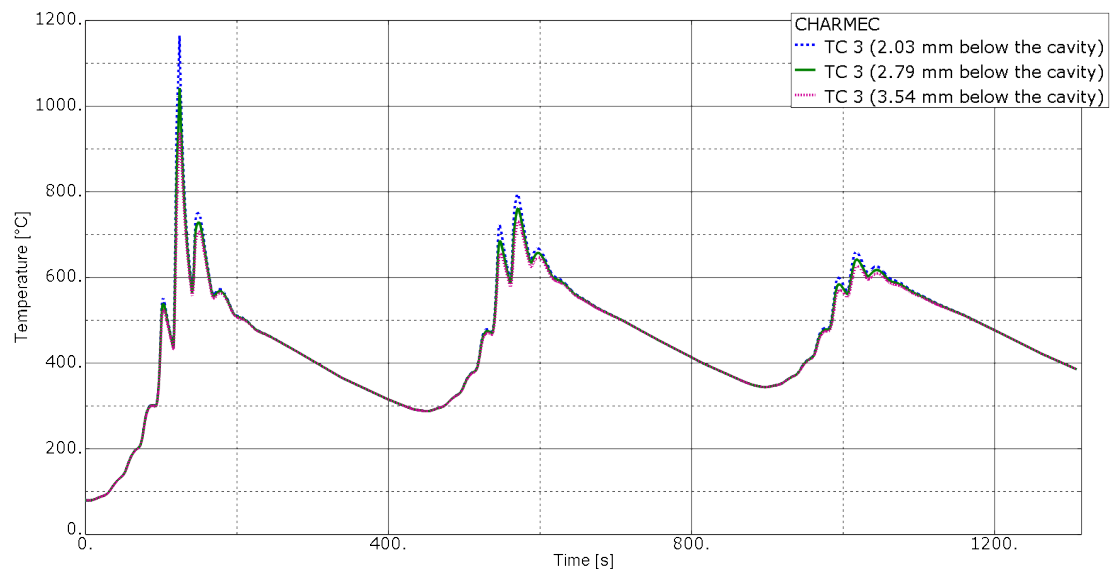


Figure 4.17 – Thermal histories for different positions in the vicinity of TC3 for a filler material temperature of 1700°C

Figure 4.17 shows that the disparity between the three curves is larger during the first pass, when the material volume between the thermocouple and the heat source is smaller. To make the graph more clear, Figure 4.18 and Figure 4.19 show zoom-ins of the first and in the second welding passes, respectively.

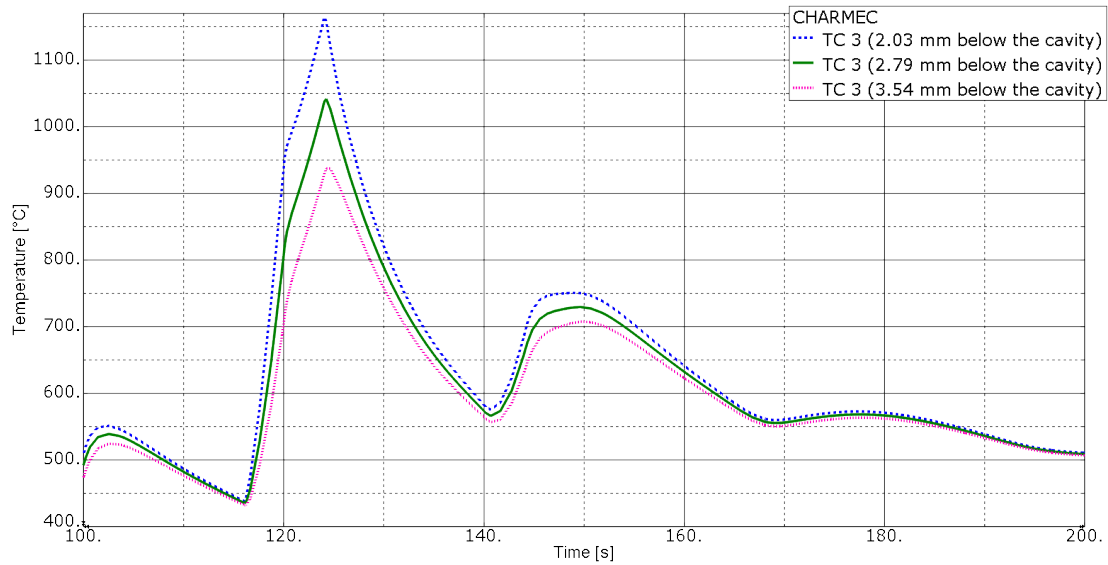


Figure 4.18 – First pass thermal history for different positions in the vicinity of TC3, for filler material temperature of 1700°C

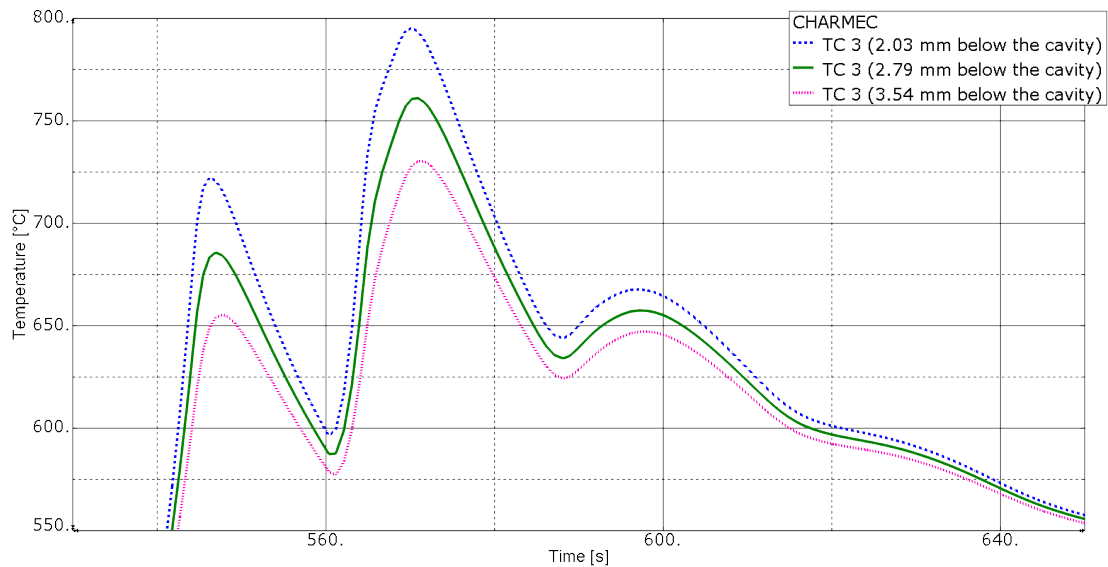


Figure 4.19 - Second pass thermal history for different positions in the vicinity of TC3, for filler material temperature of 1700°C

The same kind of study was performed for some possible locations of TC5. Here the studied position depended on both the vertical depth of the drilling and on the horizontal distance from the upper edge of the cavity. Thus, two degrees of freedom regarding the position of the analysis point were used. More information on the location of the points can be found in Table 4.3 and Figure 4.20.

Point	Drilling depth [mm]	Distance from the top cavity edge [mm]	Total distance from the cavity top corner [mm]
Point 1	5.00	2.28	5.49
Point 2	7.00	3.17	7.68
Point 3	9.43	2.03	9.65

Table 4.3 – The geometrical characteristics of the nodes used to approximate TC5

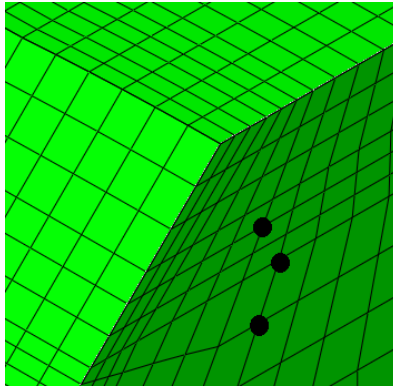


Figure 4.20 - The three analysed locations for TC5

Figure 4.21 shows the full thermal history for the three analysed locations in the vicinity of TC5, whereas Figure 4.22 to Figure 4.24 show in detail the peaks corresponding to the three passes.

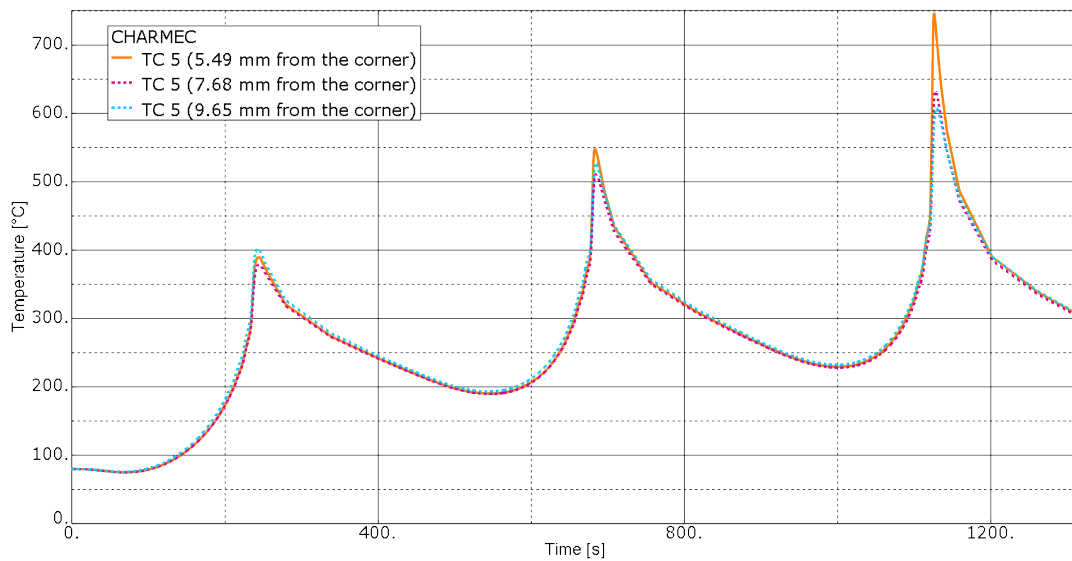


Figure 4.21 - Thermal histories for different positions in the vicinity of TC5 for a filler material temperature of 1700°C

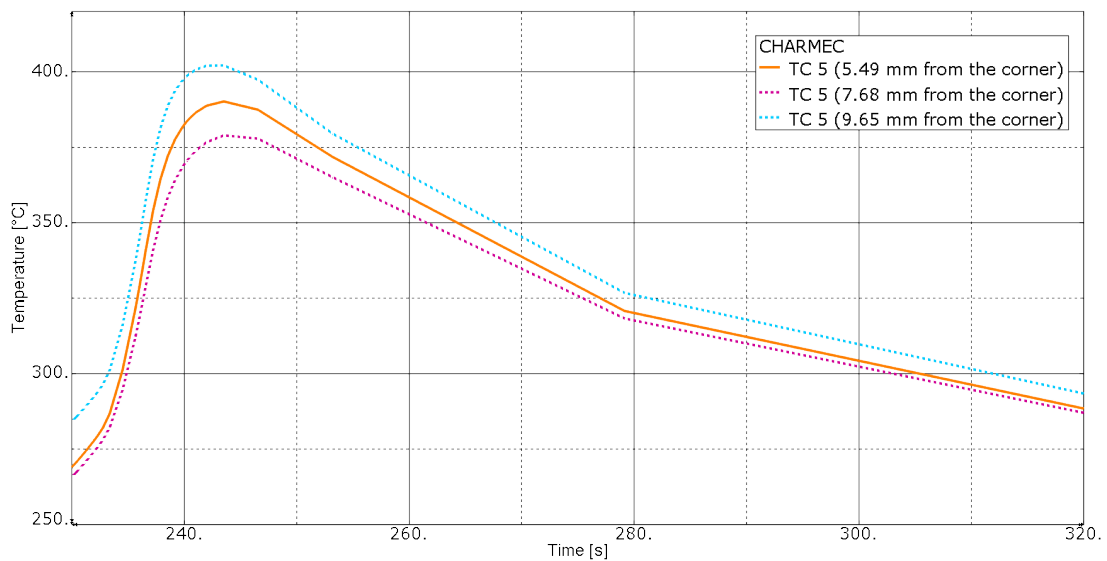


Figure 4.22 - First pass thermal history for different positions in the vicinity of TC5

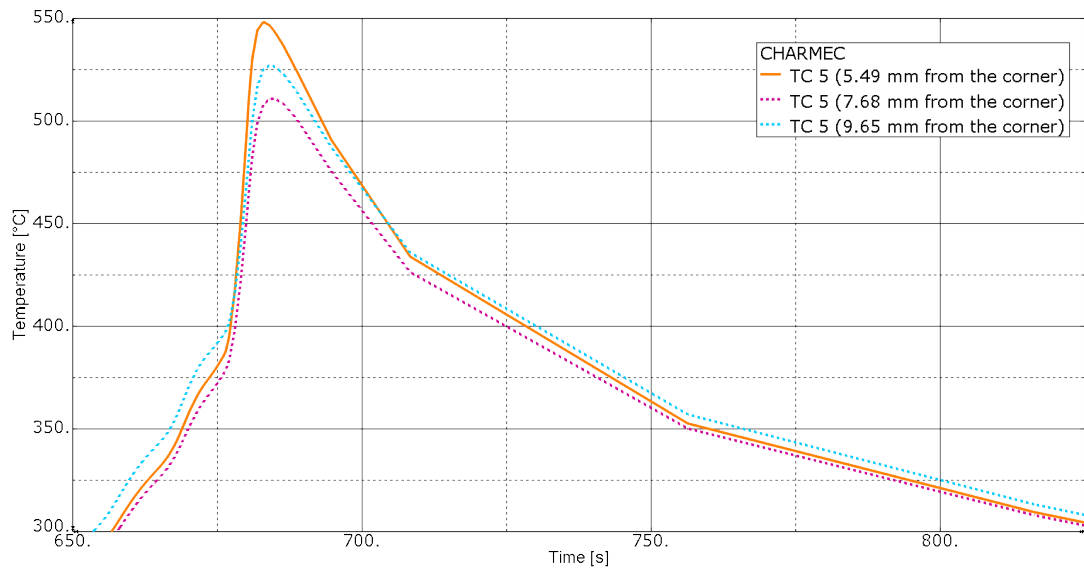


Figure 4.23 - Second pass thermal history for different positions in the vicinity of TC5

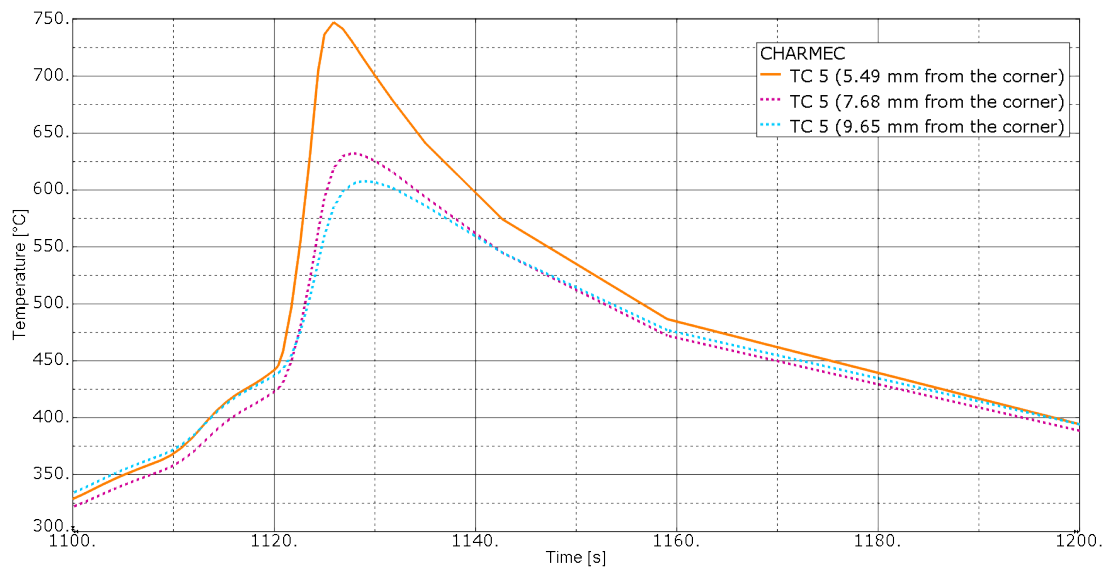


Figure 4.24 - Third pass thermal history for different positions in the vicinity of TC5

It can be noticed that in the case of the graphs referring to the temperature histories close to TC5 the location with the highest temperature was not always the same, as was the case of TC3. The magnitude of the peak indeed depended on the vertical depth of the thermocouple and the height of the deposited layer. For example, in Figure 4.22, the highest temperatures were recorded in the deepest point since the heat source was operating close to the bottom of the cavity. In Figure 4.24, on the other hand, the highest data were obtained on the most shallow point since the hot material was being laid on the top layer of the rail head.

The point which was located 7.68 mm from the cavity top corner, instead, followed a slightly different trend since it was located at a larger lateral distance from the cavity with respect to the other two test nodes. Nevertheless, the results were still within the range of the other analysed points and can therefore be considered consistent.

### 4.3.3 Influence of the corner geometry

The final step of this work focuses on the areas which were closer to the cavity corners to understand whether small changes in geometry could have any major influence on the cooling curves.

The studied points were chosen in such a way that their distance to the top cavity edge was very similar for all the analysed models (i.e. the reference geometry, the one with sharp corners and the one with rounded corners). Further, the points should be in the vicinity of the location of some thermocouples in the 2008 experiment.

The first point was in the vicinity of TC5. The position for the different cavity geometries are summarised in Table 4.4 where the drilling depth is from the running surface of the rail and the upper edge is the lateral side of the cut-out. A graphic representation of the location of the node in the case of the reference geometry is given in Figure 4.25.

Cavity corner geometry	Drilling depth [mm]	Distance from cavity top edge [mm]
Reference	7.00	3.16
Sharp	7.00	3.17
Rounded	6.99	2.94

Table 4.4 – Characteristics of the TC5 simulation points for the three geometries

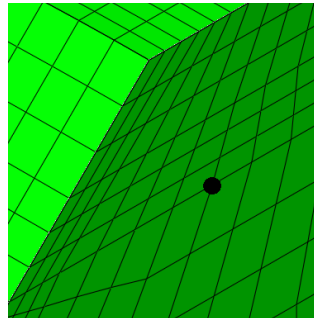


Figure 4.25 – The point used to simulate TC5 in the reference geometry

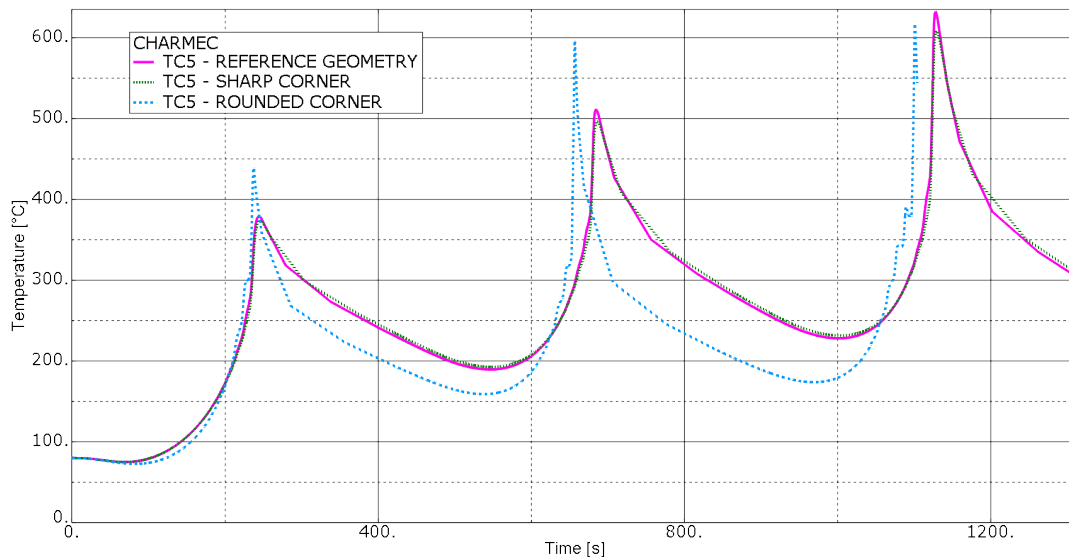


Figure 4.26 - Thermal histories in the vicinity of TC5 for different cavity corner geometries, with filler material temperature of 1700°C

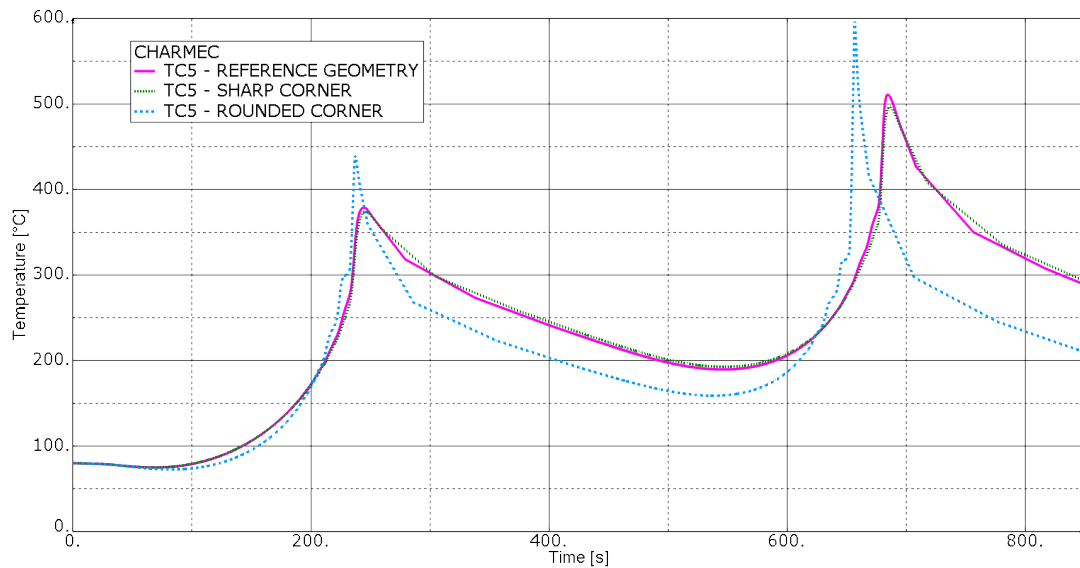


Figure 4.27 - Thermal histories in the vicinity of TC5 for the first two layers for different cavity corner geometries

Figure 4.26 and Figure 4.27 show the thermal histories at points close to TC5. It can be seen that the curves related to the reference model and to the one with the “sharp” corner follow a very similar path and their trends are hard to distinguish even in the zoomed-in version of the graphs.

The plot referred to the rounded corners model is slightly different. First of all, the time history is shifted: that is due to the fact that the variation in the cavity dimensions made the number of welding beads (and therefore the time required to complete them) slightly different.

Secondly, the peak temperatures for the first two passes in the rounded corners model are higher with respect to the other cases. That might be due to two reasons: the point of temperature evaluation in the model with the rounded corner was closer to the cavity (see Table 4.4) and the volume that the heat source had to fill in the reference and sharp corner cases was smaller than that of the circular one, see Figure 4.28, thus leading to a smaller heat input.

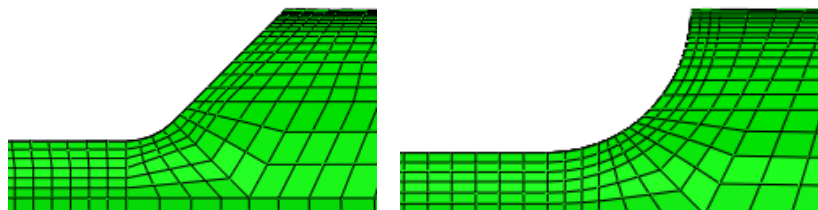


Figure 4.28 - Comparison between the corner shape in the reference geometry (left) and in the rounded one (right)

A similar comparison was done on some nodes representing TC4. Their positions with respect to the bottom of the cut-out are listed in Table 4.5 and the location in the reference geometry is depicted in Figure 4.29.

Corner geometry	Reference	Sharp	Rounded
Depth from the bottom of the cavity [mm]	2.03	2.11	2.00

Table 4.5 - Characteristics of the TC4 simulation points for the three geometries

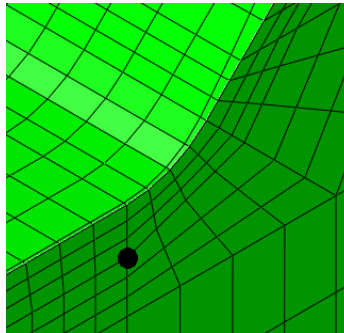


Figure 4.29 - The point used to simulate TC4 in the reference geometry analysis

The thermal history for TC4 showed its main differences in the first pass, see Figure 4.30.

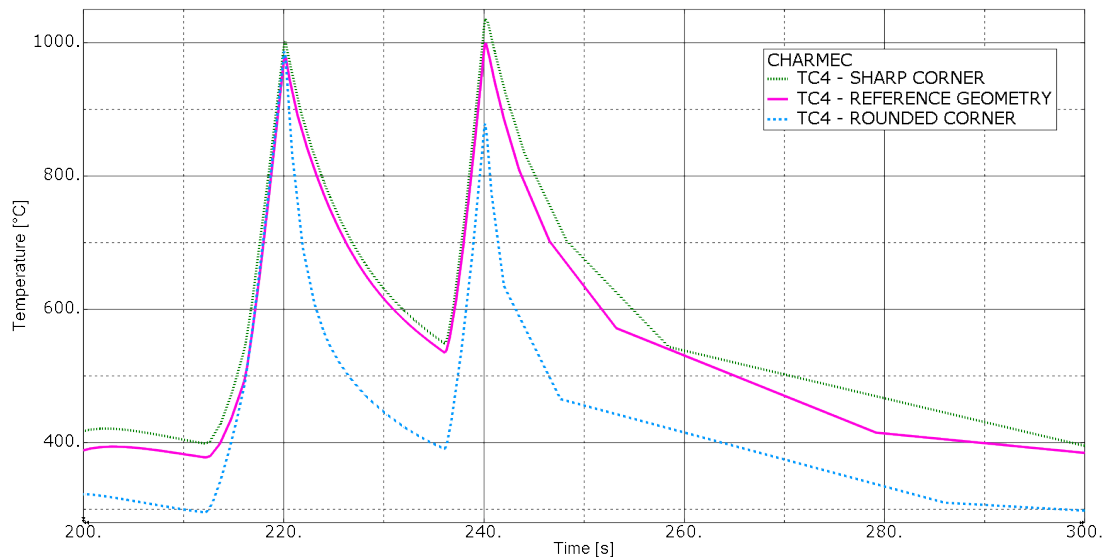


Figure 4.30 - Thermal histories for the first pass of TC4 for different corner geometries

Although the peak values for the three models were similar, the results show faster cooling rates for the rounded cavity corners model. That might be due to the fact that the curved corner geometry makes TC4 closer to the material zone which is unaffected by the welding procedure, see Figure 4.31.

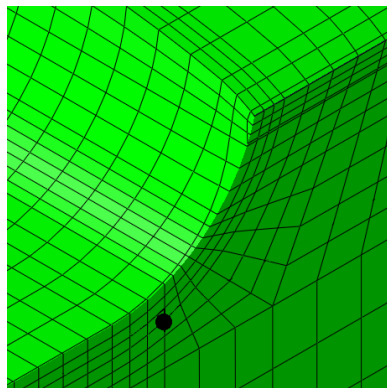


Figure 4.31 - The node representing TC4 in the rounded cavity corner model

## 5 Conclusions

The results presented in section 4 show the high potential of FE analyses in the field of heat transfer analyses applied to welding problems.

Firstly, the possibility to know the temperatures for all instants in time in every part of the repaired rail is a strong advantage. This is especially the case when (as happened in the trials held in July 2016) it is not possible to use thermocouples or similar devices during experimental processes. Another possible event that might push towards the use of numerical analyses might be the unexpected failure of the measuring equipment, as happened in the DDR experiments held in 2008. In addition, it is of course not possible to experimentally evaluate the temperatures in all points of the repaired weld even if all sensors operate as intended.

FE analyses also represent a tool to validate the metallurgical basis of the process developed by British Steel, as well. Today, preheating high carbon steels to temperatures above 343°C is considered necessary to slow down the cooling rates in the HAZ and to prevent the formation of martensite. The new DDR process tries to avoid hard microstructures by combining low preheat, optimum welding parameters and the weaved pattern [16]. Here FE-analyses are a useful tool in avoiding the difficulties in validating the new procedure by means of physical testing, which would require a very large number of samples to provide a statistically validated result. Instead, numerical simulations can be employed to verify that the formation of hard phases is not compatible with the evaluated cooling curves. Further, numerical analyses allow to test “what-if”-scenarios and thereby assess the robustness of the method.

On the other hand, simulations cannot completely take over trials and experimental results: the latter are fundamental in order to calibrate the analysis parameters and to validate the physical consistency of results. Another weak point of simulations is the necessity to make assumptions on some unclear aspects (e.g. boundary conditions, material properties) and the difficulty in taking into account all the phenomena which act during a process.

The consistency of the ways the FE-models were produced in this work was confirmed by both the results of the sensitivity analyses (see section 4.1) and the output of the different thermal histories.

As seen in section 4.3.1, the predicted temperature close to the cavity shows a clear dependency on the temperature of the filler material, thus providing a hint on the reliability of the numerical results. More in detail, an increase in the temperature of the deposited filler material (which is very hard to estimate or measure) from 1700 °C to 1800 °C resulted, during the first layer deposition, in a difference in temperature some 3.1 mm from the cavity of some 40 °C.

To further assess the validity of the numerical results, a comparison with experimental data collected in the 2008 trials was performed. As mentioned, those experiments featured a different process. On the other hand, that process is similar and the thermocouple results from the experiments the only sufficiently detailed results provided for validations.

Comparisons between experiments regarding temperature trends for layers 2 to 4 in Figure 4.12 and Figure 4.14 show similar peak values to those of simulated results for layers 1 to 3 in Figure 4.13 and Figure 4.15 when the molten material temperature is set to 1700 °C.

The most significant differences between the experimental and numerical results are the fact that in the experimental results, the peak temperatures for TC3 increase from the first to the second layer. Further, the cooling curves have different shapes where the predictions show some significant fluctuations, especially in the first passes.

The increase in peak temperatures when passing from the first to the second layer does not appear in the results of the FE model. However, provided the temperature of the applied fillet is consistent, an increase in temperature seems unlikely: Every time a welding layer is laid, the heat coming from the following layer has more material in which to be dissipated before reaching the thermocouple location. Thus, the predicted sequential decrease in peak temperatures is reasonable. However, an increase in peak temperature could occur if the welding is carried out so fast that the lower layer does not have time to cool down. As seen from the time scale of the experiment, this does not seem to be the case. The second reason could be that the conductivity is lower than assumed, which seems unlikely. A third reason could be that the preheating temperature is higher than 80°C (according to the experimental graphs, see Figure 4.12 and Figure 4.14, the area close to TC3 was preheated at about 110°C and the one close to TC5 reached a temperature of 88°C).

As for the fluctuations in the curves, these are due to the zig-zag path followed by the welding nozzle. The thermocouples are heated up when the filler material is deposited exactly above them (which is the moment that corresponds to the main peak in the graph), then the surrounding steel has some time (about 12–16 seconds, depending on the thermocouple position) to cool down before being heated up again by the deposition of a welding pass close to the location of the thermocouple. That these oscillations do not occur in the experiment measurements could be due to filtering of the measured temperature or that the process applies the filler in another pattern, but that does not seem to be the case according to the pictures in [7].

Those fluctuations are not present in the graphs referred to TC5 (Figure 4.15) as the latter is positioned after the end of the welding layer, so that the passing of the welding nozzle occurs just once per layer.

The second stage of this work, involved the study of the influence of the thermocouple position on the measured cooling curves. This study confirms the physical consistency of the simulations, as (not surprisingly) the highest temperatures occur when the heat source is close to the node where temperature is evaluated. Here it is seen that a shift in the location of temperature evaluation of 0.75 mm results in a difference in predicted (or measured) temperature for the first layer deposition in the order of 100°C. This discrepancy corresponds to a variation in the temperature of the filler material of some 200 °C.

An analysis of the influence of the detailed geometry of the cut-out and especially the corner areas revealed some interesting results. As already mentioned in section 4.3.3, the difference in the thermal history between the reference cut-out geometry and one with sharp corners is completely negligible. That can be easily explained with the

small differences in the actual geometry (see Figure 3.5 and Figure 3.7). Note that the simulations presume the fillet material to completely fill up the transition radius (or sharp corner in the case of no radius). In reality, the weld material may not completely fill a sharp corner. For that reason the geometry with a sharp corner could be unsuitable. However for simulation purposes they are as good as equivalent.

The model with the rounded geometry showed slightly different trends, but it is worth mentioning that the shape of its corners was considerably different from that of the previous two models, see Figure 3.6. The differences in temperatures can here be explained by this difference in geometry. It might also be useful to consider that such a notable variation in the geometry required a re-meshing and to the impossibility of finding a node located exactly in the same position (with respect to the heated filler material) as the ones used for the other models.

To sum up, the results obtained in the FE analyses performed in this MSc Thesis work are found to be physically consistent. The results should be of use to predict the behaviour of the steel in the heat affected zone. However, in order to improve the predictability, the model needs to be further calibrated and validated. For that reason there is a need for further experiments under controlled conditions. The thesis provides details on the experimental results that should be required for such a calibration/validation.

## 6 Future work

In general FE-analyses tend to provide results which are physically sound, but usually not fully exact. In particular for this study, some approximations were used and there are uncertainties in indata. For instance, the reliance of experimental data where the employed process is not the same as the one modelled and several parameters are unknown is not ideal. For this reason, further experimental data is required, as discussed in the conclusions. To this end, it would be wise to repeat the experimental procedure of the York experiments in June 2016, but equip the rail with thermocouples or other devices aimed at recording temperature-time curves.

Another limitation of the FE model is in the approximations which were made, especially with reference to material properties. In particular, several generic characteristic properties for low and medium carbon steels have been used. Moreover, the temperature dependency of those materials was only known up to 700 °C, while temperatures in the analysed models often reached 1700 °C. According to the way ABAQUS deals with temperature dependent material data, the values for material properties are interpolated if the analysis temperature falls within the range specified in the property definition. If the analysis temperature is below or above that interval, material properties are kept constant and respectively equal to the value at the minimum or maximum temperature in the specified interval. That implies that the material properties at 700°C were used to simulate the process where temperatures could reach values such as 1700°C. Experimental tests in order to quantify the specific properties of the welding and the rail steels on a wider temperature range would reduce the uncertainties in the numerical simulations.

The FE model can be refined by taking into account the effect that material phase transformations have on the cooling trends. This has been neglected throughout this study as no data were available on that, but including this phenomenon in more advanced FE models would make results more significant and complete.

Finally, performing the FE analyses on newer versions of the software and the welding interfaces would probably allow for a better discretisation, which might improve the accuracy somewhat.

Simulations which could be run in the future in order to better understand the effect of the investigated DDR procedure include thermomechanical analyses aimed at assessing the residual stresses in the HAZ after the material has cooled down.

Another interesting application is related to the case of the geometry with “sharp” corners. As stated in the previous sections, the differences in the thermal behaviour are not remarkable from a theoretical point of view. But, in reality, the welding procedure might not completely fill the sharp corners and some voids might form when the cooling process starts. Analysis that accounts for this phenomenon might provide a deeper knowledge on the relationship between the corner geometry, the cooling behaviour and the risk of weld defects.

## 7 Acknowledgements

The work performed within this Master Thesis is part of the Work Package 3.1 of the EU project In2Rail. The help of the following people and partners was fundamental for the completion of this work:

Jay Jaiswal, from ARR Rail Solutions Ltd and the Institute of Railway Research of the University of Huddersfield, who gave us feedback during the conference calls and provided us with literature and reports on repair welding procedures and in particular on the DDR method that is studied in this work.

Sandra Fretwell-Smith, from British Steel Ltd, who handed over the material data and some hints on how to approximate the real properties of the rail base and weld steels.

Stefan Kallander from Trafikverket.

The supervisor Elena Kabo and the examiner Anders Ekberg, the people at CHARMEC and at the department of Applied Mechanics of Chalmers University of Technology who shared opinions, material and information with me.

Finally, it is worth mentioning that this MSc Thesis project was carried within the Erasmus+ bilateral agreement between Chalmers University of Technology and Politecnico di Torino.

## References

1. Jaiswal J. *Scope of Proposed Demonstration Trials*. EU project In2Rail report. Institute of Railway Research, University of Huddersfield, Huddersfield, United Kingdom, 8 pp, 2016
2. Jaiswal J. *Repair of Rail Head Defects – Status of Current Techniques*. EU project In2Rail report. Institute of Railway Research, University of Huddersfield, Huddersfield, United Kingdom, 19 pp, 2016
3. Grassie S L. Squats and squat-type defects in rails: the understanding to date. *Journal of Rail and Rapid Transit*, vol 226, p 235–242, 2011
4. NSW Transport RailCorp. *Rail Defects Handbook*, version 1.2, RailCorp Engineering manual, Sydney, Australia, 83 pp, 2012
5. UIC Code 712, *Rail Defects*, Union Internationale des Chemins de fer, Paris, France, 111 pp, 2002
6. Frick A, *BVH 524.100 – Katalog över rälsfel* (Catalogue of rail defects), Trafikverket, Borlänge, Sweden, 115 pp, 2015 (in Swedish)
7. Jaiswal J. *Cost Effective Repair of Rail Surface Defects – A Proposal for Demonstration of Developed Technology*. ARR Rail Solutions Ltd, Huddersfield, United Kingdom, 20 pp, 2016
8. Jaiswal J. *Repair of Rail Head Defects – Available Technologies*. IRR Report EU-I2R/31-01, Institute of Railway Research, University of Huddersfield, Huddersfield, United Kingdom, 8 pp, 2015
9. Frick A, *TDOK 2013:0393 Banöverbyggnad – Spårsvetsning* (Track structure – rail welding), Trafikverket, Borlänge, Sweden, 19 pp, 2015 (in Swedish)
10. Johnson R S. *The Repair of Discrete Rail Defects – Analysis of the method developed by ARR*. INFERRICITY Ltd, Doc. ref. V01-13-06-16, Derby, United Kingdom, 23 pp, 2016
11. Fretwell-Smith S, Zhu C. *Evaluation of welding feasibility of head repair welds*. Document number BritishSteelRD\_12, British Steel Ltd, Scunthorpe, United Kingdom, 31 pp, 2016
12. ABAQUS. *ABAQUS/Standard*, version 6.14, Dassault Systèmes Simulia Corp., Providence, USA, 2014
13. ABAQUS, *ABAQUS extension for welding simulations*, Dassault Systèmes Simulia Corp., Providence, USA, 2012
14. Jerath V, Smith H, Jaiswal J. *Discrete Defect Repair – A Novel Process*. TATA Steel Ltd and Corus Group, 15<sup>th</sup> technical meeting of the Institute of Rail Welding, Power Point presentation, 27 slides, 2009
15. Frick A, *BVH 524.12 – Måttuppgifter för räler och tungämnen. Standardprofiler samt äldre och utgångna profiler* (Dimensions for rails and switch blades. Standard, older and discarded profiles), Trafikverket, Borlänge, Sweden, 43 pp, 2015 (in Swedish)
16. Jaiswal J. *Personal communication on the shape of the cavity, on the filler material and on the experimental procedures*. ARR Rail Solutions Ltd, Huddersfield, United Kingdom, 2017

17. Fretwell-Smith S. *Personal communication on material properties regarding the rail material and the weld consumable*. British Steel Ltd, Scunthorpe, United Kingdom, 2017
18. ESAB. *Welding Handbook. Consumables for manual and automatic welding*, Eighth edition, ESAB North America, USA, 529 pp, 2016
19. Hlavaty I, Sigmund M, Krejčí L, Mohyla P. The bainitic steels for rails applications. *Materials Engineering*, vol 16, no 4, p 44–50, 2009
20. Andersson E, Berg M, Stichel S. *Rail Vehicle Dynamics*. Division of Rail Vehicles, Kungliga Tekniska Högskolan, Stockholm, Sweden, 2007
21. Liu G R, Quek S S. *The Finite Element Method, A Practical Course – Second Edition*. Butterworth-Heinemann, Waltham, United States, 421 pp, 2015
22. Wen S. *Modelling rail head repair welding*. TATA Steel Ltd, Project number 11205-01, London, United Kingdom, 27 pp, 2015
23. Wen S, Smith H. *Modelling of heat affected zone cooling rates during the repair welding of grooved rail*. TATA Steel Ltd., Project number 7855/03, London, United Kingdom, 19 pp, 2010
24. Bray D P, Leggatt N A, Dennis R J, Smith M C, Bouchard P J. *Numerical Methods For Welding Simulation – The Next Technical Step*. Frazer-Nash Consultancy Ltd and British Energy Generation Ltd for the SIMULIA 2009 Customer Conference, United Kingdom, 15 pp, 2009

## Appendix A – Sensitivity analysis

As anticipated in Section 4.1, the results regarding the sensitivity analysis on the other two nodal points (the “central” and the “right” ones) are presented in this appendix.

### A1 Central Point

The “central node”, here referred as “SA-C”, was located exactly at the centre of the cavity, with respect to both the longitudinal and the lateral directions of the rail. Its depth from the bottom of the milled surface was 2.03 mm, see Figure A.1.

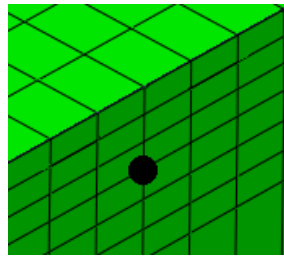


Figure A.1 – The position of SA-C node

Table A.1 summarises the main points of the thermal history for the FE-node SA-C:

Moment	Time instant [s]	Temperatures [°C] and Mesh			coarse-medium difference [%]	medium-fine difference [%]
		coarse	medium	fine		
1st peak	128	734,8	723,3	722,6	1,57	0,10
1st minimum	442	198,4	193,2	192,2	2,62	0,52
2nd peak	562	555,6	542,5	542,6	2,36	0,02
2nd minimum	888	221,6	215,3	214,3	2,84	0,46
3rd peak	1007	490,9	476,9	475,7	2,85	0,25
3rd minimum	1308	239,7	232,1	231,3	3,17	0,34

Table A.1 – Temperature values for the nodal point SA-C for the three different meshes

The temperature trend for the SA-C FE-node is depicted in Figure A.2. Figure A.3 represents the thermal history for the first layer deposition for SA-C.

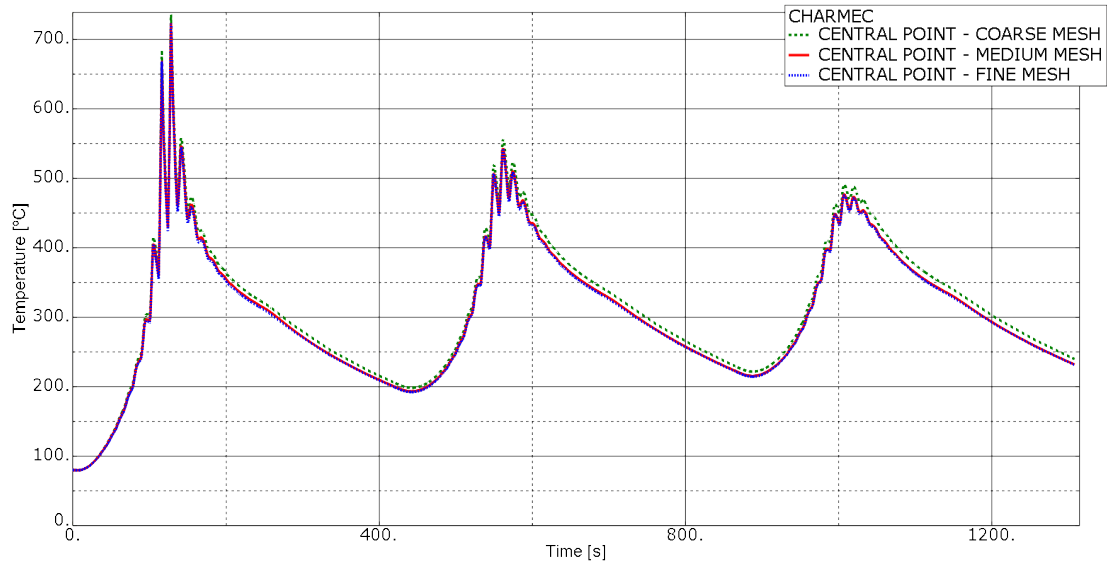


Figure A.2 – Thermal history for SA-C node for the three meshes

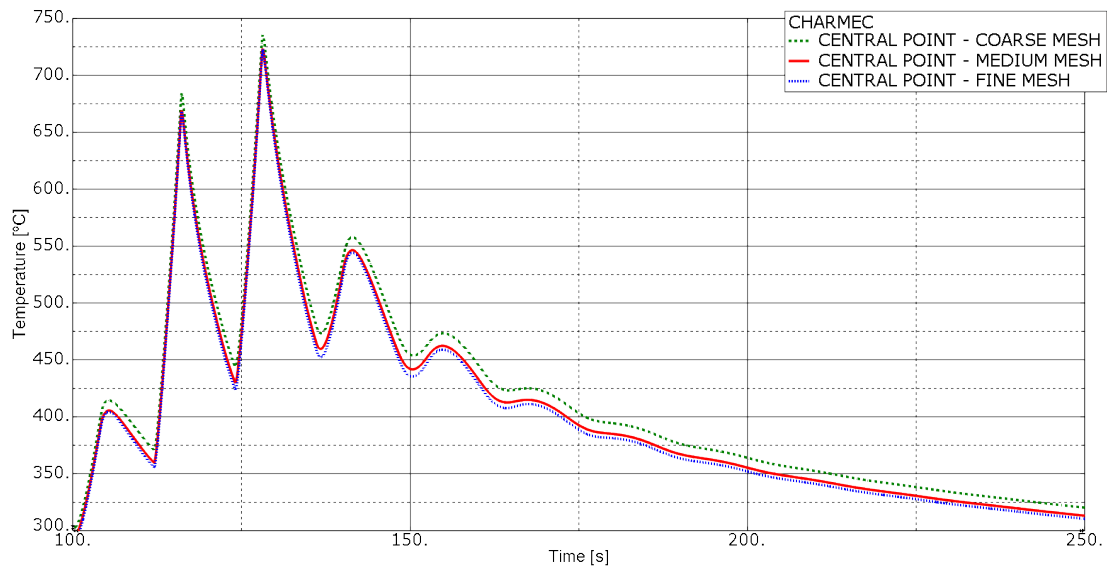


Figure A.3 – Comparison of the time histories evaluated using the three meshes in SA-C node for the time associated to the first layer deposition

## A2 Right point

The “right node”, here referred as “SA-R”, was located close to the corner where the deposition of the three layers ends, at a depth of 7 mm, which is comparable to the one of the interface between the first and the second layer and along the longitudinal plane of the rail, see Figure A.4.

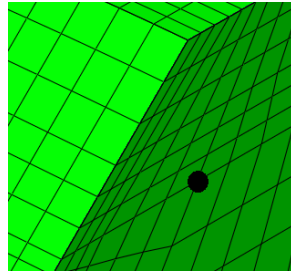


Figure A.4 - The position of SA-R node

The main points of its thermal history for the different meshes are shown in Table A.2:

Moment	Time instant [s]	Temperatures [°C] and mesh			coarse-medium difference [%]	medium-fine difference [%]
		coarse	medium	fine		
1st peak	240	317,4	308,6	306,4	2,77	0,71
1st minimum	533	137,1	133,8	133,1	2,41	0,52
2nd peak	682	429,7	416,8	415,4	3,00	0,34
2nd minimum	979	155,9	151,8	151,1	2,63	0,46
3rd peak	1126	512,8	502,5	502,6	2,01	0,02
3rd minimum	1308	239,7	232,1	231,3	3,17	0,34

Table A.2 - Temperature values for the nodal point SA-R for the three different meshes

The temperature trend for SA-R node is depicted in Figure A.5. Figure A.6 represents the thermal history for the first layer deposition for SA-C node.

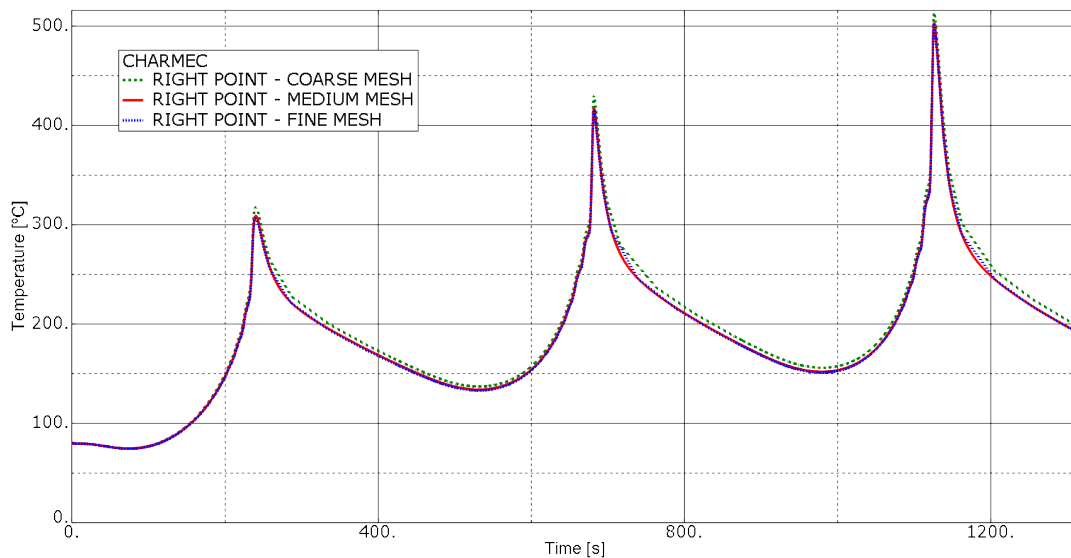


Figure A.5 - Thermal history for SA-R node for the three meshes

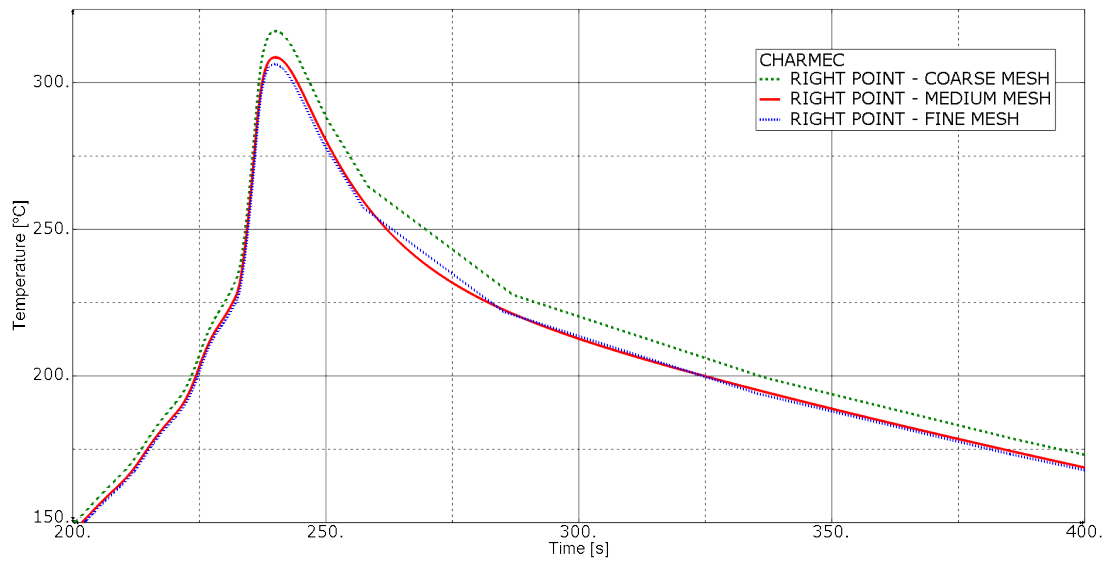


Figure A.6 - Comparison of the time histories evaluated using the three meshes in SA-R node for the time associated to the first layer deposition

The results in Table A.1 and Table A.2 confirm the ones obtained in section 4.1. The difference in output between the coarse and the medium mesh is in between 2% and 3%, whereas the one between the medium and the fine mesh is again around 0.4%.

The same trend is witnessed in Figure A.2 to Figure A.6, which confirm the results discussed in section 4.1.